RJ Lee*Group*, Inc.

350 Hochberg Road • Monroeville, PA 15146
412/325-1776 • FAX 412/733-1799

March 21, 1995

Mr. Christopher Salerno
Municipality of Anchorage
Department of Health & Human Services
825 "L" Street, Room 501
P.O. Box 196650
Anchorage, AL 99519-6650

RE: CCSEM Analysis of Ten PM-10 Quartz Filters
RJ Lee Group Project No. ESH503033
Municipality of Anchorage DHHS Purchase Order No. 47159

Dear Mr. Salerno:

Attached you will find a summary of the analytical results for ten PM-10 quartz filter samples which we received on February 24, 1995 (reference your letter to Gary Casuccio dated February 22, 1995). The samples were collected from volcanic episodes in the Anchorage area. Table I summarizes the identification and general appearance of the samples.

The objective of this study was to characterize the particle matter associated with each sample and provide information on particle size and composition. Computer-controlled scanning electron microscopy (CCSEM) was used to provide the requested information. The PM-10 quartz filter samples were prepared using our standard techniques involving the redeposition of particulate matter onto a polycarbonbate filter and analyzing by CCSEM.

Table II summarizes the particle type data for each sample. Figures 1 through 4 provide examples of typical particle types. A more detailed summary of the CCSEM data is attached to this report. Tables A and E report the relative abundance of the various particle species detected during the analysis and their average composition. Table B presents the actual number of particles analyzed at various size ranges. The remaining tables summarize the size, mass and aerodynamic mass distributions. The size and mass distributions are based on average physical diameter and the aerodynamic mass distribution are based on calculated aerodynamic equivalent diameter.

Figure 5 provides log plots of the cumulative number percent of selected samples (i.e., 5/20/94, 11/21/93 and 8/19/92). Figure 6 provides cumulative mass distribution based on physical diameters and aerodynamic equivalent diameter of these same samples.

These results are submitted pursuant to RJ Lee Group's current terms and conditions of sale, including the company's standard warranty and limitation of liability provisions. No responsibility or liability is assumed for the manner in which the results are used or interpreted. Unless notified in writing to return the samples covered by this report, RJ Lee Group will store them for a period of thirty (30) days before discarding.

Should you have any questions regarding this information, please do not hesitate to contact me.

Sincerely,

Guangxiang Jin for

G. S. Casuccio
Vice President
Environmental Services

GSC:dls
Attachments

TABLE I

IDENTIFICATION AND DESCRIPTION OF PM-10 SAMPLES

Municipality of Anchorage
Department of Health and Human Services

DHHS Sample ID	Sample Site	Sample Date	Sample Conc. ($\mu g/m^3$)	RJ Lee Group Sample No.	General Appearance & Stereoscopic Review
Filter #2662285	26A	7/1/92	35	607051	The glass-fiber filter is gray in color. Moderate-to-heavy loading of fine black particulate matter.
Filter #3549395	26C	5/20/93	54	607052	The glass-fiber filter is gray in color. Heavy loading of fine black particulate matter.
Filter #4594955	26C	5/12/94	57	607053	The glass-fiber filter is gray in color. Heavy loading of fine black particulate matter.
Filter #9662609	26B	5/12/92	80	607054	The glass-fiber filter is dark gray in color. Very heavy loading of fine black, gray and transparent particulate matter.
Filter #3549877	26D	11/2/93	82	607055	The glass-fiber filter is dark gray in color. Very heavy loading of fine black, gray and transparent particulate matter.
Filter #4594899	26B	4/24/94	83	607056	The glass-fiber filter is gray in color. Heavy loading of fine black particulate matter.
Filter #9662453	26D	8/28/92	128	607057	The glass-fiber filter is gray in color. Heavy loading of fine gray particulate matter. Moderate loading of fine black particulate matter.
Filter #3549235	26C	3/25/93	131	607058	The glass-fiber filter is brownish gray in color. Very heavy loading of fine gray particulate matter. Moderate loading of fine black particulate matter.
Filter #4594778	26C	2/17/94	198	607059	The glass-fiber filter is dark brownish gray in color. Very heavy loading of brownish gray particulate matter.
Filter #9662426	26D	8/19/92	305	607060	The glass-fiber filter is tan in color. Heavy loading of tan particulate matter. Moderate loading of dark brown-to-black particulate matter.
Filter #2662956	—	—	—	607061	The glass-fiber filter is white in color. Very light loading. Small amount of black particles observed.

TABLE II

SUMMARY OF CCSEM PARTICLE TYPE RESULTS, WT. % (NUM. %)

Municipality of Anchorage
Department of Health and Human Services

Particle Type	7/1/92	5/20/93	5/12/94	5/12/92	11/2/93
Si-rich	13.1 (13.9)	15.0 (13.2)	16.4 (18.9)	13.8 (8.1)	18.7 (13.7)
Si/Al-rich (mixed clays)	77.6 (3.3)	71.2 (11.6)	76.7 (27.5)	84.4 (37.1)	77.7 (46.7)
Ca-rich	2.8 (0.2)	3.5 (67.1)	3.3 (0.4)	0.9 (1.6)	0.9 (2.7)
Fe-rich	2.6 (0.2)	2.5 (1.5)	1.4 (1.7)	0.5 3.3)	1.9 (4.8)
C-rich	3.2 (81.4)	0.1 (6.7)	1.4 (51.4)	0.4 (47.6)	0.8 (31.0)
Miscellaneous	0.7 (1.0)	7.7 (<0.1)	0.8 (0.1)	<0.1 (2.3)	<0.1 (1.1)

Particle Type	4/24/94	8/28/92	3/25/93	2/17/94	8/19/92
Si-rich	16.4 (14.6)	7.5 (8.4)	11.6 (13.9)	17.1 (13.0)	4.7 (9.2)
Si/Al-rich (mixed clays)	79.1 (18.3)	86.0 (26.3)	80.0 (31.5)	76.0 (27.0)	90.8 (34.8)
Ca-rich	0.8 (0.5)	0.6 (0.9)	3.8 (1.1)	2.4 (1.2)	1.0 (0.4)
Fe-rich	2.5 (1.6)	0.8 (0.7)	0.8 (1.3)	1.2 (0.8)	2.1 (0.6)
C-rich	1.3 (65.0)	5.0 (62.1)	0.9 (52.0)	3.2 (57.2)	1.3 (54.2)
Miscellaneous	— —	0.1 (1.6)	2.9 (<0.1)	<0.1 (0.8)	0.2 (0.8)

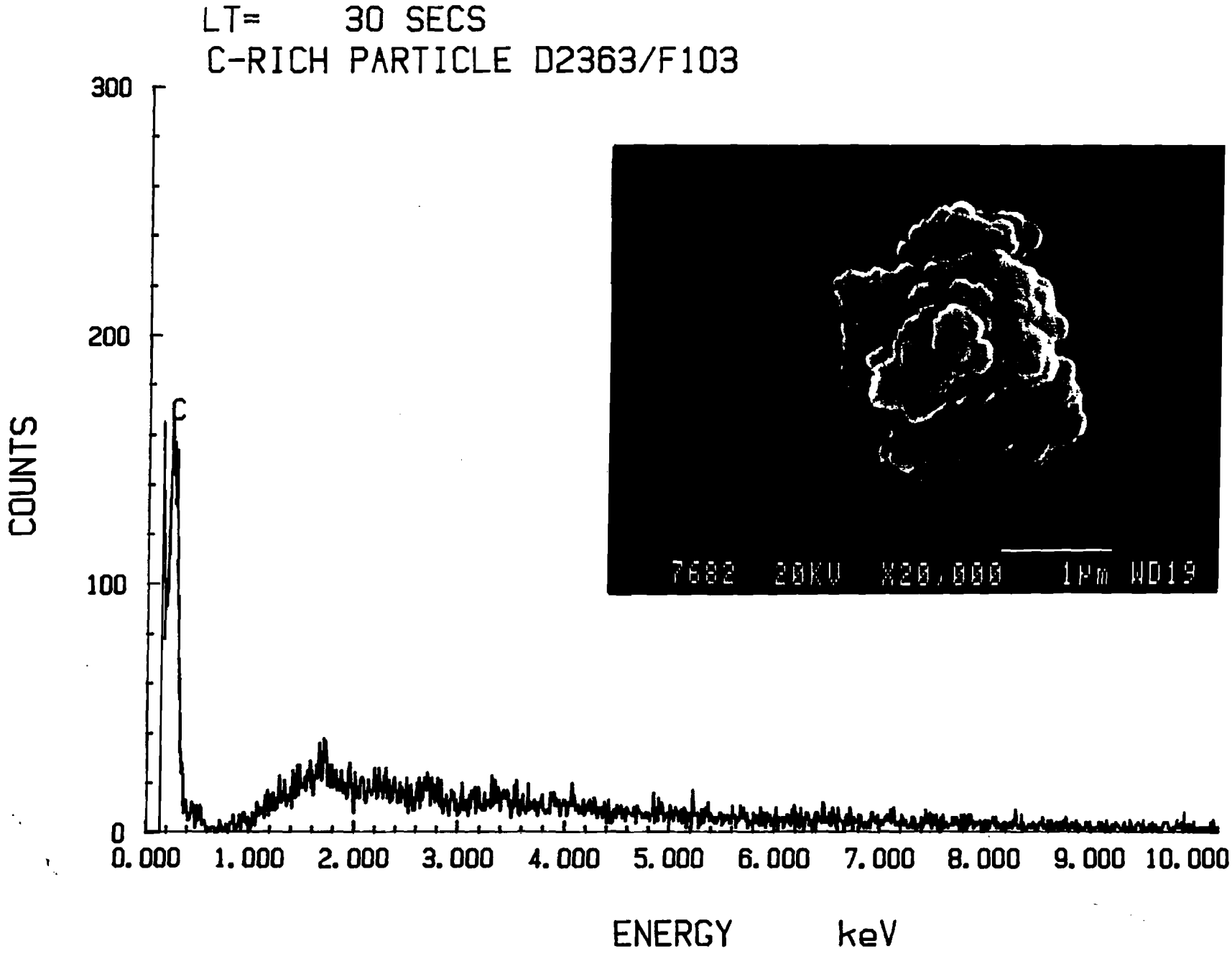
LT= 30 SECS
C-RICH PARTICLE D2363/F103
300
200
100
0
COUNTS
C
7682 20KV X20,000 1Pm WD19
0.000
1.000
2.000
3.000
4.000
5.000
6.000
7.000
8.000
9.000
10.000
ENERGY keV

Figure 1

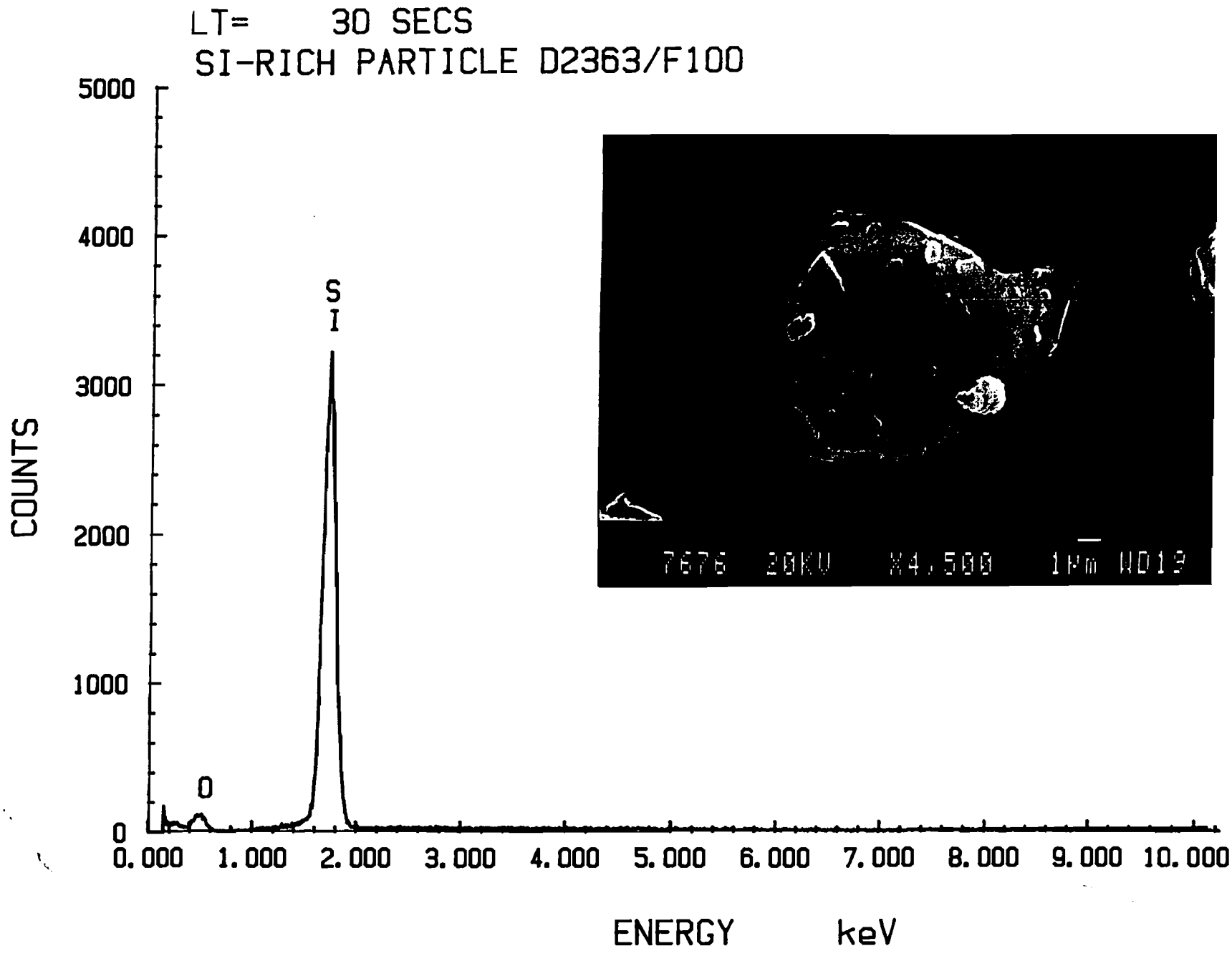
LT= 30 SECS
SI-RICH PARTICLE D2363/F100
5000
4000
3000
2000
1000
0
COUNTS
S
I
O
0.000
1.000
2.000
3.000
4.000
5.000
6.000
7.000
8.000
9.000
10.000
ENERGY keV
7676 20KV X4,500 1μm WD19

Figure 2

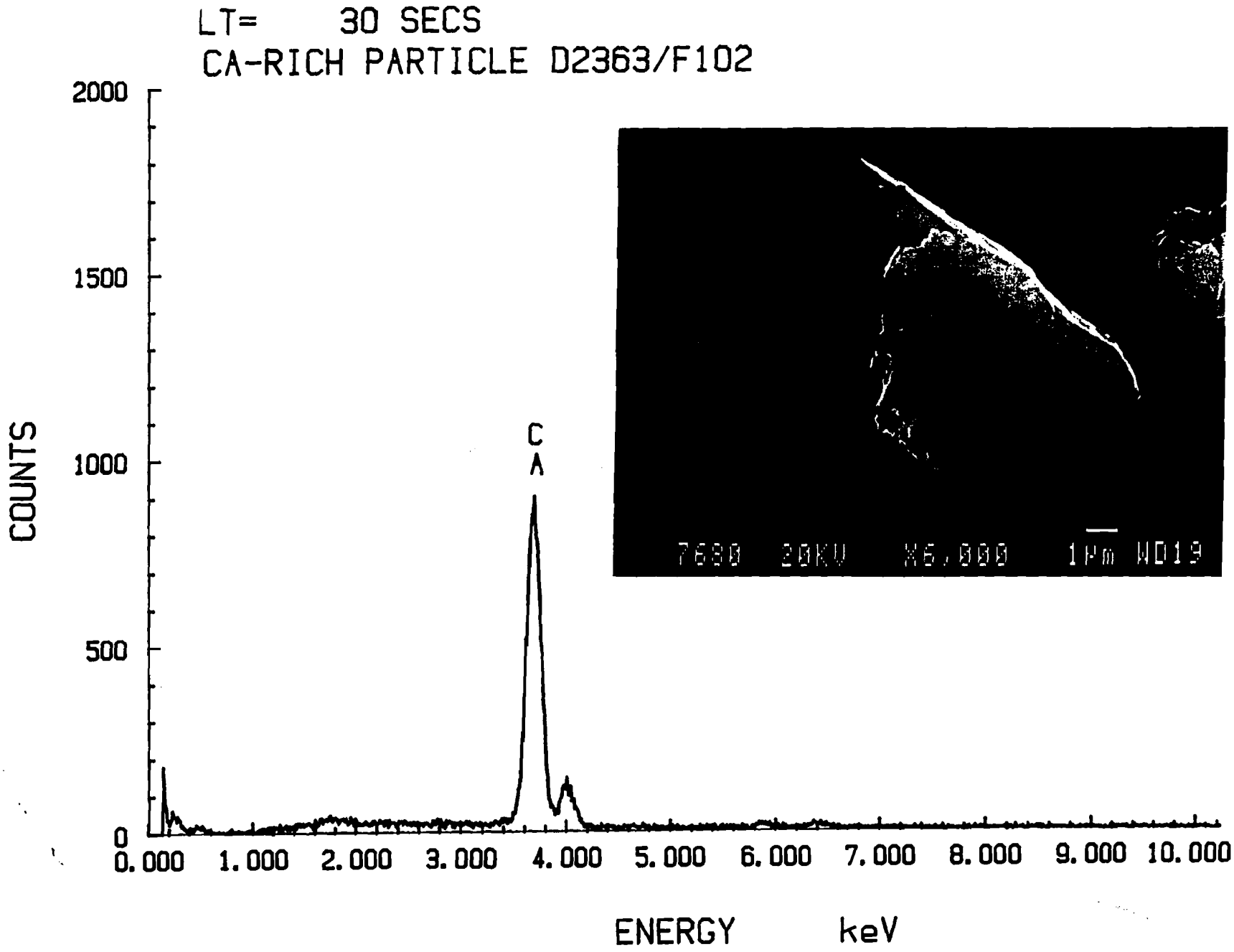
LT= 30 SECS
CA-RICH PARTICLE D2363/F102
2000
1500
1000
500
0
COUNTS
C
A
7680 20KV X6,000 1Pm WD19
0.000
1.000
2.000
3.000
4.000
5.000
6.000
7.000
8.000
9.000
10.000
ENERGY keV

Figure 3

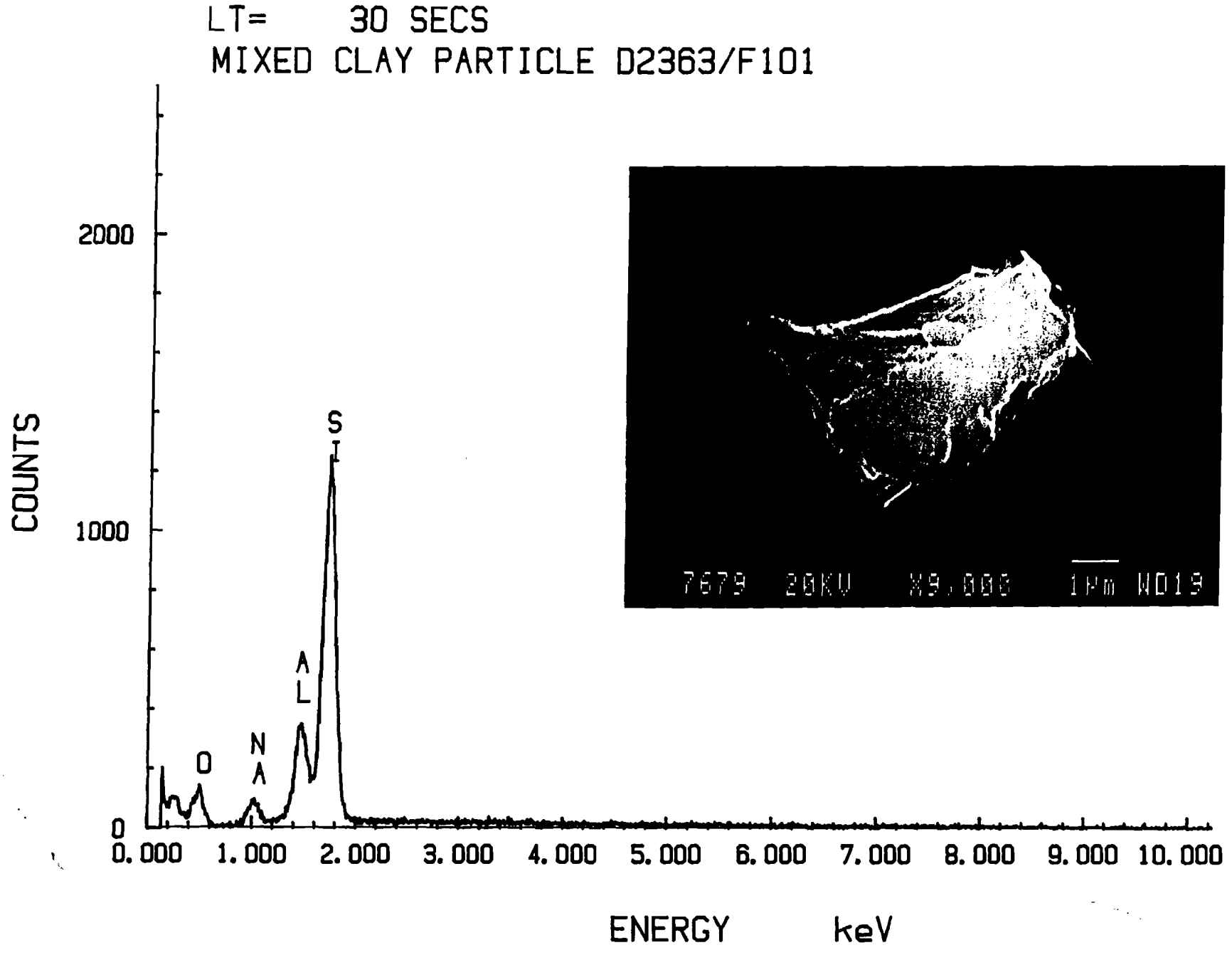
LT= 30 SECS
MIXED CLAY PARTICLE D2363/F101
COUNTS
2000
1000
0
O
N
A
A
L
S
0.000
1.000
2.000
3.000
4.000
5.000
6.000
7.000
8.000
9.000
10.000
ENERGY keV
7679 20KV X9,000 1μm WD19

Figure 4

MUNICIPALITY of ANCHORAGE
Department of Health and Human Service

RJ Lee Group Project No. ESH503033

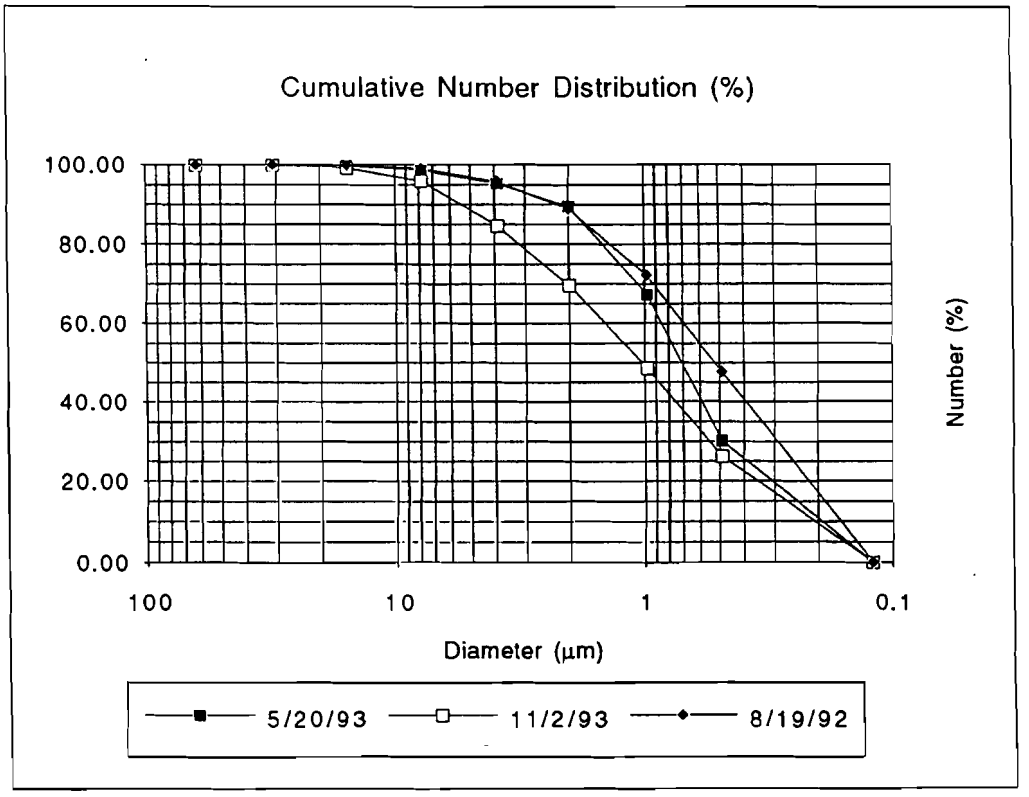

Figure 5

MUNICIPALITY of ANCHORAGE
Department of Health and Human Service

RJ Lee Group Project No. ESH503033

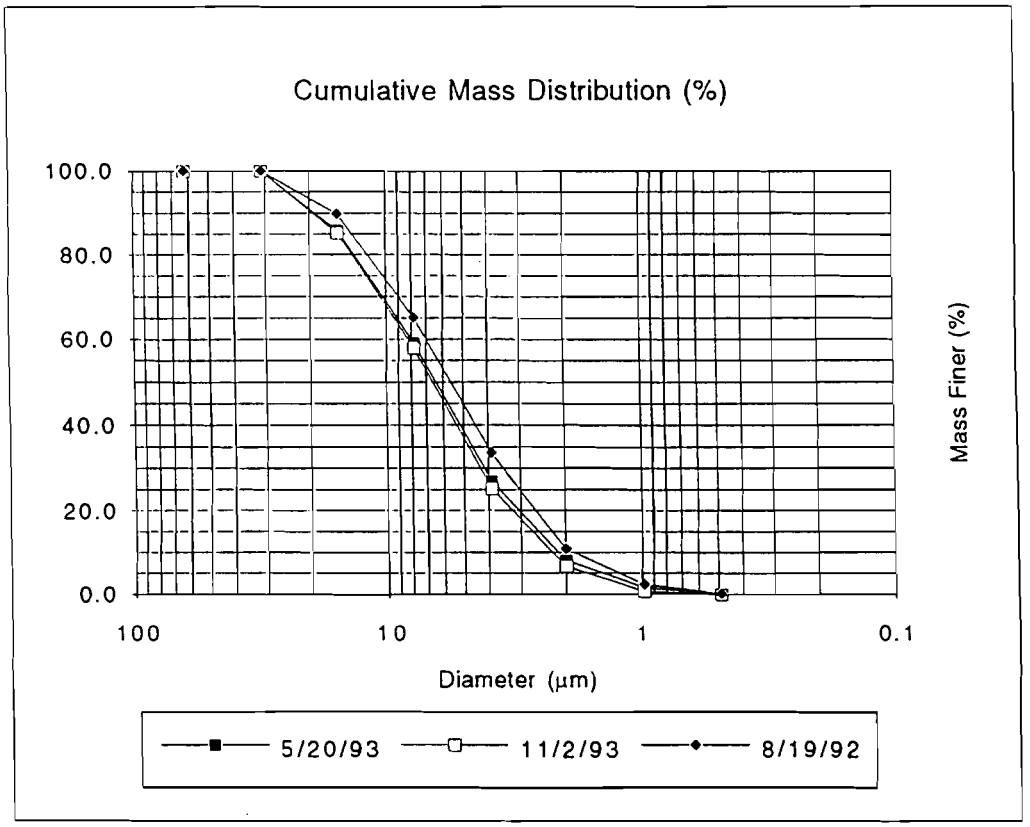

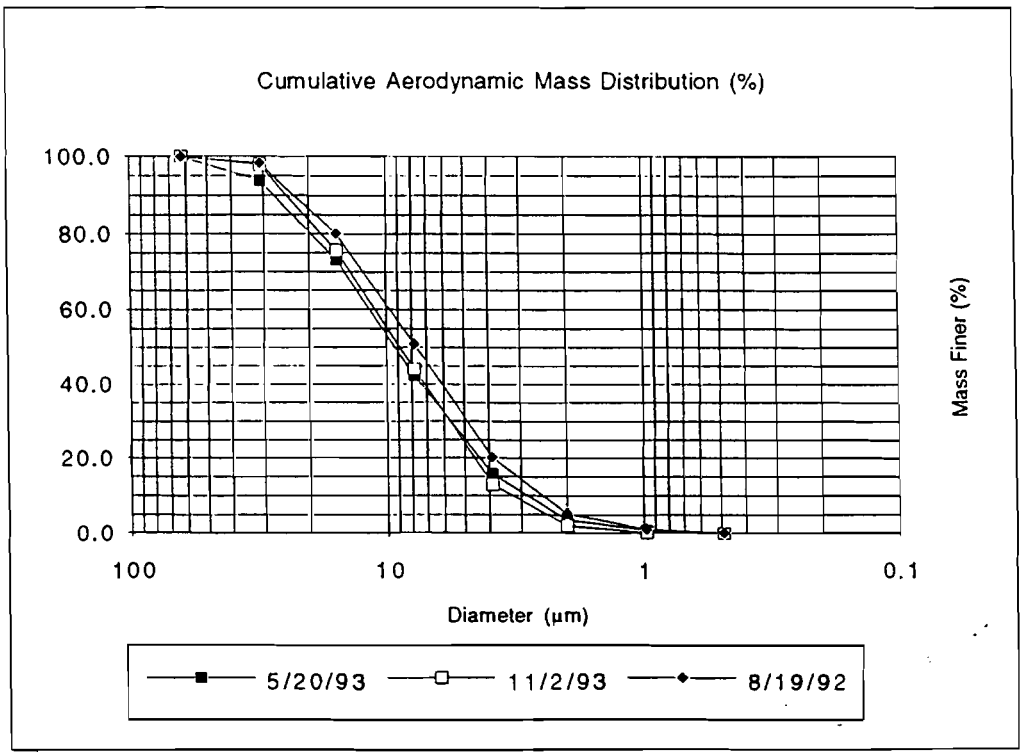

Figure 6

Client_Name	MOA-DHHS
Client_Number	PM10#35
Project_Number	ESH503033
Sample_Number	607051
Analysis_Date	3/15/95
Instrument	JSM-840

Mag	Fields	particles
200	4.559	200
400	4.059	198
800	0.279	99

Classes	#	Number %	Wt %	Ave. size
C-rich	88	81.44	3.21	0.4
Si-rich	114	13.86	13.08	0.7
Ca-rich	14	0.18	2.79	2.5
Fe-rich	19	0.24	2.63	2.0
Mixed clay	260	3.32	77.61	2.4
Misc	2	0.97	0.68	0.8
Totals	497	100.00	100.00	0.5

Table A

Number Distribution by Average Diameter (microns)

		0.2 -	2.5 -	5.0 -	10.0 -	15.0 -	20.0 -	25.0 -
Classes	Number	2.5	5.0	10.0	15.0	20.0	25.0	30.0
C-rich	88	84	0	3	1	0	0	0
Si-rich	114	72	25	14	3	0	0	0
Ca-rich	14	6	5	3	0	0	0	0
Fe-rich	19	12	6	1	0	0	0	0
Mixed clay	260	71	89	84	15	1	0	0
Misc	2	1	1	0	0	0	0	0
Totals	497	246	126	105	19	1	0	0

Table B

Size Distribution by Average Diameter (microns)

		0.2 -	2.5 -	5.0 -	10.0 -	15.0 -	20.0 -	25.0 -
Classes	Number %	2.5	5.0	10.0	15.0	20.0	25.0	30.0
C-rich	81.4	100.0	0.0	0.0	0.0	0.0	0.0	0.0
Si-rich	13.9	98.0	1.5	0.4	0.1	0.0	0.0	0.0
Ca-rich	0.2	55.1	38.8	6.1	0.0	0.0	0.0	0.0
Fe-rich	0.2	83.7	14.7	1.6	0.0	0.0	0.0	0.0
Mixed clay	3.3	64.4	24.4	9.4	1.7	0.1	0.0	0.0
Misc	1.0	99.6	0.4	0.0	0.0	0.0	0.0	0.0
Totals	100.0	98.4	1.1	0.4	0.1	0.0	0.0	0.0

Table C

Client_Name	MOA-DHHS
Client_Number	PM10#35
Project_Number	ESH503033
Sample_Number	607051
Analysis_Date	3/15/95
Instrument	JSM-840

Mass Distribution by Average Diameter (microns)

		0.2 - 2.5	2.5 - 5.0	5.0 - 10.0	10.0 - 15.0	15.0 - 20.0	20.0 - 25.0	25.0 - 30.0
Classes	Mass %	2.5	5.0	10.0	15.0	20.0	25.0	30.0
C-rich	3.2	40.7	0.0	22.2	37.1	0.0	0.0	0.0
Si-rich	13.1	11.8	19.7	37.6	30.8	0.0	0.0	0.0
Ca-rich	2.8	4.7	20.6	74.6	0.0	0.0	0.0	0.0
Fe-rich	2.6	17.1	44.1	38.8	0.0	0.0	0.0	0.0
Mixed clay	77.6	2.7	13.8	44.7	33.9	4.9	0.0	0.0
Misc	0.7	19.0	81.0	0.0	0.0	0.0	0.0	0.0
Totals	100.0	5.7	15.6	43.5	31.5	3.8	0.0	0.0

Table D

Aerodynamic Mass Distribution by Aerodynamic Diameter (microns)

		0.2 - 2.5	2.5 - 5.0	5.0 - 10.0	10.0 - 15.0	15.0 - 20.0	20.0 - 25.0	25.0 - 30.0
Classes	Mass %	2.5	5.0	10.0	15.0	20.0	25.0	30.0
C-rich	3.2	40.7	0.0	22.2	37.1	0.0	0.0	0.0
Si-rich	13.1	8.3	13.1	29.4	49.2	0.0	0.0	0.0
Ca-rich	2.8	1.8	20.7	2.9	74.6	0.0	0.0	0.0
Fe-rich	2.6	2.8	14.3	44.1	38.8	0.0	0.0	0.0
Mixed clay	77.6	0.9	7.0	22.9	40.5	16.5	12.3	0.0
Misc	0.7	19.0	0.0	0.0	81.0	0.0	0.0	0.0
Totals	100.0	3.3	8.1	23.5	42.7	12.8	9.5	0.0

Table E

Average Composition

Classes	#	C	O	NA	MG	AL	SI	P	S	CL	K	CA	TI	CR	MN	FE	NI	CU	ZN	AS	PB
C-rich	88	96	0	0	0	0	1	0	2	0	0	0	0	0	0	0	0	0	0	0	0
Si-rich	114	34	2	0	0	0	60	0	0	0	0	0	0	0	0	2	0	1	0	0	0
Ca-rich	14	0	0	0	0	6	5	4	16	2	0	63	2	0	0	0	0	0	0	0	0
Fe-rich	19	0	3	0	0	1	7	0	3	0	0	1	1	0	0	85	0	0	0	0	0
Mixed clay	260	16	2	0	0	24	46	0	0	0	2	4	0	0	0	5	0	0	0	0	0
Misc	2	49	0	0	0	14	0	0	0	0	0	0	0	0	0	0	0	36	0	0	0
Totals	497	84	0	0	0	1	11	0	1	0	0	0	0	0	0	1	0	0	0	0	0

Table F

Client_Name	MOA-DHHS
Client_Number	PM10#54
Project_Number	ESH503033
Sample_Number	607052
Analysis_Date	3/15/95
Instrument	JSM-840

Mag	Fields	particles
200	1.968	200
400	1.722	200
800	0.605	98

Classes	#	Number %	Wt %	Ave. size
C-rich	8	6.70	0.07	0.6
Si-rich	100	13.16	14.96	1.3
Ca-rich	118	67.10	3.51	0.6
Fe-rich	11	1.46	2.50	1.4
Mixed clay	260	11.57	71.18	2.8
Misc	1	0.02	7.77	14.9
Totals	498	100.00	100.00	1.0

Table A

Number Distribution by Average Diameter (microns)

		0.2 - 2.5	2.5 - 5.0	5.0 - 10.0	10.0 - 15.0	15.0 - 20.0	20.0 - 25.0	25.0 - 30.0
Classes	Number							
C-rich	8	8	0	0	0	0	0	0
Si-rich	100	50	32	17	1	0	0	0
Ca-rich	118	109	5	4	0	0	0	0
Fe-rich	11	5	6	0	0	0	0	0
Mixed clay	260	64	99	91	6	0	0	0
Misc	1	0	0	0	1	0	0	0
Totals	498	236	142	112	8	0	0	0

Table B

Size Distribution by Average Diameter (microns)

		0.2 - 2.5	2.5 - 5.0	5.0 - 10.0	10.0 - 15.0	15.0 - 20.0	20.0 - 25.0	25.0 - 30.0
Classes	Number %							
C-rich	6.7	100.0	0.0	0.0	0.0	0.0	0.0	0.0
Si-rich	13.2	86.0	11.8	2.1	0.1	0.0	0.0	0.0
Ca-rich	67.1	99.6	0.3	0.1	0.0	0.0	0.0	0.0
Fe-rich	1.5	77.6	22.4	0.0	0.0	0.0	0.0	0.0
Mixed clay	11.6	53.9	32.6	12.7	0.8	0.0	0.0	0.0
Misc	0.0	0.0	0.0	0.0	100.0	0.0	0.0	0.0
Totals	100.0	92.2	5.8	1.8	0.1	0.0	0.0	0.0

Table C

Client_Name MOA-DHHS
Client_Number PM10#54
Project_Number ESH503033
Sample_Number 607052
Analysis_Date 3/15/95
Instrument JSM-840

Mass Distribution by Average Diameter (microns)

		0.2 -	2.5 -	5.0 -	10.0 -	15.0 -	20.0 -	25.0 -
Classes	Mass %	2.5	5.0	10.0	15.0	20.0	25.0	30.0
C-rich	0.1	100.0	0.0	0.0	0.0	0.0	0.0	0.0
Si-rich	15.0	8.4	33.6	36.0	22.0	0.0	0.0	0.0
Ca-rich	3.5	43.2	21.7	35.1	0.0	0.0	0.0	0.0
Fe-rich	2.5	8.0	92.0	0.0	0.0	0.0	0.0	0.0
Mixed clay	71.2	4.0	23.9	54.5	17.7	0.0	0.0	0.0
Misc	7.8	0.0	0.0	0.0	100.0	0.0	0.0	0.0
Totals	100.0	5.9	25.1	45.4	23.6	0.0	0.0	0.0

Table D

Aerodynamic Mass Distribution by Aerodynamic Diameter (microns)

		0.2 -	2.5 -	5.0 -	10.0 -	15.0 -	20.0 -	25.0 -
Classes	Mass %	2.5	5.0	10.0	15.0	20.0	25.0	30.0
C-rich	0.1	100.0	0.0	0.0	0.0	0.0	0.0	0.0
Si-rich	15.0	4.2	24.7	39.9	9.2	22.0	0.0	0.0
Ca-rich	3.5	38.8	16.4	33.0	11.8	0.0	0.0	0.0
Fe-rich	2.5	2.7	15.0	82.3	0.0	0.0	0.0	0.0
Mixed clay	71.2	0.8	10.7	41.7	34.0	12.8	0.0	0.0
Misc	7.8	0.0	0.0	0.0	0.0	0.0	100.0	0.0
Totals	100.0	2.7	12.3	38.9	26.0	12.4	7.8	0.0

Table E

Average Composition

Classes	#	C	O	NA	MG	AL	SI	P	S	CL	K	CA	TI	CR	MN	FE	NI	CU	ZN	AS	PB
C-rich	8	81	0	0	0	0	0	0	20	0	0	0	0	0	0	0	0	0	0	0	0
Si-rich	100	10	1	0	0	0	85	0	2	0	0	1	0	0	0	1	0	0	0	0	0
Ca-rich	118	14	0	0	0	0	0	0	34	0	0	52	0	0	0	0	0	0	0	0	0
Fe-rich	11	0	1	0	0	0	8	0	2	0	0	2	0	0	0	87	0	0	0	0	0
Mixed clay	260	3	3	0	1	22	59	0	0	0	1	4	0	0	0	7	0	0	0	0	0
Misc	1	0	4	0	3	6	20	0	0	0	0	4	59	0	0	4	0	0	0	0	0
Totals	498	16	0	0	0	3	18	0	24	0	0	36	0	0	0	2	0	0	0	0	0

Table F

Client_Name	MOA-DHHS
Client_Number	PM10#57
Project_Number	ESH503033
Sample_Number	607053
Analysis_Date	3/16795
Instrument	JSM-840

Mag	Fields	particles
200	5.832	200
400	3.517	200
800	2.197	99

Classes	#	Number %	Wt %	Ave. size
C-rich	91	51.41	1.43	0.5
Si-rich	100	18.93	16.44	1.1
Ca-rich	7	0.42	3.27	3.2
Fe-rich	10	1.68	1.41	1.5
Mixed clay	288	27.50	76.68	2.1
Misc	3	0.05	0.77	5.1
Totals	499	100.00	100.00	1.1

Table A

Number Distribution by Average Diameter (microns)

Classes	Number	0.2 - 2.5	2.5 - 5.0	5.0 - 10.0	10.0 - 15.0	15.0 - 20.0	20.0 - 25.0	25.0 - 30.0
C-rich	91	83	7	1	0	0	0	0
Si-rich	100	40	33	27	0	0	0	0
Ca-rich	7	2	3	1	1	0	0	0
Fe-rich	10	8	1	1	0	0	0	0
Mixed clay	288	84	109	89	6	0	0	0
Misc	3	0	2	1	0	0	0	0
Totals	499	217	155	120	7	0	0	0

Table B

Size Distribution by Average Diameter (microns)

Classes	Number %	0.2 - 2.5	2.5 - 5.0	5.0 - 10.0	10.0 - 15.0	15.0 - 20.0	20.0 - 25.0	25.0 - 30.0
C-rich	51.4	99.0	1.0	0.0	0.0	0.0	0.0	0.0
Si-rich	18.9	87.2	10.3	2.5	0.0	0.0	0.0	0.0
Ca-rich	0.4	55.5	36.1	4.2	4.2	0.0	0.0	0.0
Fe-rich	1.7	92.1	6.9	1.0	0.0	0.0	0.0	0.0
Mixed clay	27.5	64.9	29.1	5.6	0.4	0.0	0.0	0.0
Misc	0.1	0.0	66.7	33.3	0.0	0.0	0.0	0.0
Totals	100.0	87.0	10.8	2.1	0.1	0.0	0.0	0.0

Table C

Client_Name MOA-DHHS
Client_Number PM10#57
Project_Number ESH503033
Sample_Number 607053
Analysis_Date 3/16/95
Instrument JSM-840

Mass Distribution by Average Diameter (microns)

		0.2 -	2.5 -	5.0 -	10.0 -	15.0 -	20.0 -	25.0 -
Classes	Mass %	2.5	5.0	10.0	15.0	20.0	25.0	30.0
C-rich	1.4	44.8	39.6	15.5	0.0	0.0	0.0	0.0
Si-rich	16.4	8.0	31.8	60.1	0.0	0.0	0.0	0.0
Ca-rich	3.3	6.6	16.2	0.6	76.6	0.0	0.0	0.0
Fe-rich	1.4	43.8	28.3	27.8	0.0	0.0	0.0	0.0
Mixed clay	76.7	6.2	35.2	46.3	12.2	0.0	0.0	0.0
Misc	0.8	0.0	53.6	46.4	0.0	0.0	0.0	0.0
Totals	100.0	7.5	34.2	46.4	11.9	0.0	0.0	0.0

Table D

Aerodynamic Mass Distribution by Aerodynamic Diameter (microns)

		0.2 -	2.5 -	5.0 -	10.0 -	15.0 -	20.0 -	25.0 -
Classes	Mass %	2.5	5.0	10.0	15.0	20.0	25.0	30.0
C-rich	1.4	33.9	50.6	15.5	0.0	0.0	0.0	0.0
Si-rich	16.4	2.5	21.8	49.5	26.2	0.0	0.0	0.0
Ca-rich	3.3	0.0	18.7	4.7	0.0	0.0	76.6	0.0
Fe-rich	1.4	6.1	37.7	28.3	27.8	0.0	0.0	0.0
Mixed clay	76.7	1.2	20.1	46.2	21.2	11.3	0.0	0.0
Misc	0.8	0.0	0.0	53.6	46.4	0.0	0.0	0.0
Totals	100.0	1.9	20.9	44.8	21.3	8.7	2.5	0.0

Table E

Average Composition

Classes	#	C	O	NA	MG	AL	SI	P	S	CL	K	CA	TI	CR	MN	FE	NI	CU	ZN	AS	PB
C-rich	91	93	1	0	0	1	3	0	0	0	0	0	0	0	0	0	0	0	0	0	0
Si-rich	100	34	5	0	0	0	59	0	0	0	0	0	1	0	0	0	0	0	0	0	0
Ca-rich	7	0	8	0	4	0	10	20	2	0	0	55	0	0	0	0	0	0	1	0	0
Fe-rich	10	6	6	0	2	1	7	0	8	0	0	1	5	0	0	65	0	0	0	0	0
Mixed clay	288	11	6	1	1	17	48	0	0	0	2	4	0	0	0	9	0	0	0	0	0
Misc	3	0	0	0	0	1	4	0	0	2	0	1	60	0	0	0	0	31	0	0	0
Totals	499	58	3	0	0	5	26	0	0	0	1	2	0	0	0	4	0	0	0	0	0

Table F

Client_Name	MOA-DHHS
Client_Number	PM10#80
Project_Number	ESH503033
Sample_Number	607054
Analysis_Date	3/16/95
Instrument	JSM-840

Mag	Fields	particles
200	1.227	200
400	1.341	200
800	1.130	100

Classes	#	Number %	Wt %	Ave. size
C-rich	86	47.55	0.41	0.4
Si-rich	75	8.14	13.75	2.5
Ca-rich	11	1.62	0.93	1.5
Fe-rich	13	3.32	0.49	1.2
Mixed clay	310	37.13	84.38	2.3
Misc	5	2.23	0.05	0.7
Totals	500	100.00	100.00	1.3

Table A

Number Distribution by Average Diameter (microns)

Classes	Number	0.2 - 2.5	2.5 - 5.0	5.0 - 10.0	10.0 - 15.0	15.0 - 20.0	20.0 - 25.0	25.0 - 30.0
C-rich	86	81	5	0	0	0	0	0
Si-rich	75	21	30	24	0	0	0	0
Ca-rich	11	6	4	1	0	0	0	0
Fe-rich	13	13	0	0	0	0	0	0
Mixed clay	310	107	101	94	8	0	0	0
Misc	5	5	0	0	0	0	0	0
Totals	500	233	140	119	8	0	0	0

Table B

Size Distribution by Average Diameter (microns)

Classes	Number %	0.2 - 2.5	2.5 - 5.0	5.0 - 10.0	10.0 - 15.0	15.0 - 20.0	20.0 - 25.0	25.0 - 30.0
C-rich	47.6	99.0	1.0	0.0	0.0	0.0	0.0	0.0
Si-rich	8.1	54.3	34.6	11.0	0.0	0.0	0.0	0.0
Ca-rich	1.6	82.3	15.4	2.3	0.0	0.0	0.0	0.0
Fe-rich	3.3	100.0	0.0	0.0	0.0	0.0	0.0	0.0
Mixed clay	37.1	67.2	22.5	9.5	0.8	0.0	0.0	0.0
Misc	2.2	100.0	0.0	0.0	0.0	0.0	0.0	0.0
Totals	100.0	83.3	11.9	4.5	0.3	0.0	0.0	0.0

Table C

Client_Name	MOA-DHHS
Client_Number	PM10#80
Project_Number	ESH503033
Sample_Number	607054
Analysis_Date	3/16/95
Instrument	JSM-840

Mass Distribution by Average Diameter (microns)

		0.2 - 2.5	2.5 - 5.0	5.0 - 10.0	10.0 - 15.0	15.0 - 20.0	20.0 - 25.0	25.0 - 30.0
Classes	Mass %	2.5	5.0	10.0	15.0	20.0	25.0	30.0
C-rich	0.4	54.8	45.2	0.0	0.0	0.0	0.0	0.0
Si-rich	13.7	3.5	27.3	69.2	0.0	0.0	0.0	0.0
Ca-rich	0.9	16.5	55.3	28.2	0.0	0.0	0.0	0.0
Fe-rich	0.5	100.0	0.0	0.0	0.0	0.0	0.0	0.0
Mixed clay	84.4	3.4	17.7	56.8	22.1	0.0	0.0	0.0
Misc	0.0	100.0	0.0	0.0	0.0	0.0	0.0	0.0
Totals	100.0	4.3	19.4	57.7	18.7	0.0	0.0	0.0

Table D

Aerodynamic Mass Distribution by Aerodynamic Diameter (microns)

		0.2 - 2.5	2.5 - 5.0	5.0 - 10.0	10.0 - 15.0	15.0 - 20.0	20.0 - 25.0	25.0 - 30.0
Classes	Mass %	2.5	5.0	10.0	15.0	20.0	25.0	30.0
C-rich	0.4	44.1	25.8	30.2	0.0	0.0	0.0	0.0
Si-rich	13.7	2.1	16.0	60.3	21.6	0.0	0.0	0.0
Ca-rich	0.9	2.0	14.5	83.5	0.0	0.0	0.0	0.0
Fe-rich	0.5	28.7	71.3	0.0	0.0	0.0	0.0	0.0
Mixed clay	84.4	1.1	8.5	35.2	35.4	19.8	0.0	0.0
Misc	0.0	100.0	0.0	0.0	0.0	0.0	0.0	0.0
Totals	100.0	1.6	10.0	38.8	32.9	16.7	0.0	0.0

Table E

Average Composition

Classes	#	C	O	NA	MG	AL	SI	P	S	CL	K	CA	TI	CR	MN	FE	NI	CU	ZN	AS	PB
C-rich	86	89	1	0	0	1	5	0	0	0	0	1	1	0	0	0	0	0	0	0	0
Si-rich	75	16	5	0	0	0	77	0	0	0	0	0	0	0	0	1	0	0	0	0	0
Ca-rich	11	29	5	0	0	3	13	1	8	0	0	34	6	0	0	0	0	0	0	0	0
Fe-rich	13	16	5	0	0	1	9	0	4	0	0	2	0	0	0	61	0	0	0	0	0
Mixed clay	310	16	6	1	1	15	47	0	0	0	3	4	0	0	0	7	0	0	0	0	0
Misc	5	41	3	0	0	0	7	0	3	0	1	4	8	1	0	1	0	29	2	0	0
Totals	500	51	4	0	0	6	27	0	1	0	1	2	1	0	0	5	0	1	0	0	0

Table F

Client_Name	MOA-DHHS
Client_Number	PM10#82
Project_Number	ESH503033
Sample_Number	607055
Analysis_Date	3/16/95
Instrument	JSM-840

Mag	Fields	particles
200	1.295	200
400	1.422	200
800	1.947	99

Classes	#	Number %	Wt %	Ave. size
C-rich	67	30.98	0.84	0.6
Si-rich	81	13.66	18.69	2.1
Ca-rich	12	2.73	0.87	1.4
Fe-rich	17	4.84	1.93	1.2
Mixed clay	320	46.71	77.67	2.6
Misc	2	1.07	0.00	0.5
Totals	499	100.00	100.00	1.8

Table A

Number Distribution by Average Diameter (microns)

		0.2 - 2.5	2.5 - 5.0	5.0 - 10.0	10.0 - 15.0	15.0 - 20.0	20.0 - 25.0	25.0 - 30.0
Classes	Number							
C-rich	67	62	3	2	0	0	0	0
Si-rich	81	26	28	25	2	0	0	0
Ca-rich	12	7	5	0	0	0	0	0
Fe-rich	17	11	3	3	0	0	0	0
Mixed clay	320	96	123	95	6	0	0	0
Misc	2	2	0	0	0	0	0	0
Totals	499	204	162	125	8	0	0	0

Table B

Size Distribution by Average Diameter (microns)

		0.2 - 2.5	2.5 - 5.0	5.0 - 10.0	10.0 - 15.0	15.0 - 20.0	20.0 - 25.0	25.0 - 30.0
Classes	Number %							
C-rich	31.0	98.3	1.3	0.3	0.0	0.0	0.0	0.0
Si-rich	13.7	66.0	24.0	9.2	0.7	0.0	0.0	0.0
Ca-rich	2.7	85.9	14.1	0.0	0.0	0.0	0.0	0.0
Fe-rich	4.8	85.5	11.4	3.1	0.0	0.0	0.0	0.0
Mixed clay	46.7	54.4	34.7	10.3	0.6	0.0	0.0	0.0
Misc	1.1	100.0	0.0	0.0	0.0	0.0	0.0	0.0
Totals	100.0	72.5	20.8	6.3	0.4	0.0	0.0	0.0

Table C

Client_Name	MOA-DHHS
Client_Number	PM10#82
Project_Number	ESH503033
Sample_Number	607055
Analysis_Date	3/16/95
Instrument	JSM-840

Mass Distribution by Average Diameter (microns)

		0.2 -	2.5 -	5.0 -	10.0 -	15.0 -	20.0 -	25.0 -
Classes	Mass %	2.5	5.0	10.0	15.0	20.0	25.0	30.0
C-rich	0.8	13.8	27.9	58.4	0.0	0.0	0.0	0.0
Si-rich	18.7	2.0	17.7	61.2	19.1	0.0	0.0	0.0
Ca-rich	0.9	16.9	83.1	0.0	0.0	0.0	0.0	0.0
Fe-rich	1.9	11.4	24.9	63.6	0.0	0.0	0.0	0.0
Mixed clay	77.7	3.4	23.8	58.3	14.5	0.0	0.0	0.0
Misc	0.0	100.0	0.0	0.0	0.0	0.0	0.0	0.0
Totals	100.0	3.5	23.2	58.4	14.8	0.0	0.0	0.0

Table D

Aerodynamic Mass Distribution by Aerodynamic Diameter (microns)

		0.2 -	2.5 -	5.0 -	10.0 -	15.0 -	20.0 -	25.0 -
Classes	Mass %	2.5	5.0	10.0	15.0	20.0	25.0	30.0
C-rich	0.8	13.8	27.9	58.4	0.0	0.0	0.0	0.0
Si-rich	18.7	0.7	12.8	34.9	42.1	9.5	0.0	0.0
Ca-rich	0.9	10.5	32.5	56.9	0.0	0.0	0.0	0.0
Fe-rich	1.9	3.8	19.7	54.0	22.5	0.0	0.0	0.0
Mixed clay	77.7	1.0	13.3	35.9	39.3	6.3	4.2	0.0
Misc	0.0	100.0	0.0	0.0	0.0	0.0	0.0	0.0
Totals	100.0	1.2	13.7	36.4	38.8	6.7	3.3	0.0

Table E

Average Composition

Classes	#	C	O	NA	MG	AL	SI	P	S	CL	K	CA	TI	CR	MN	FE	NI	CU	ZN	AS	PB
C-rich	67	89	2	0	0	1	5	0	1	1	1	0	0	0	0	0	0	0	0	0	0
Si-rich	81	21	5	0	0	0	73	0	0	1	0	0	0	0	0	0	0	0	0	0	0
Ca-rich	12	16	5	0	1	1	7	10	2	0	0	52	5	0	0	0	0	0	2	0	0
Fe-rich	17	13	5	0	0	3	10	0	9	0	0	1	0	0	0	59	0	0	0	0	0
Mixed clay	320	8	6	1	2	16	51	0	0	0	2	7	0	0	0	8	0	0	0	0	0
Misc	2	18	0	0	0	1	1	0	12	20	0	0	0	0	0	0	0	47	0	0	0
Totals	499	35	5	0	1	8	36	0	1	1	1	5	0	0	0	7	0	1	0	0	0

Table F

Client_Name	MOA-DHHS
Client_Number	PM10#83
Project_Number	ESH503033
Sample_Number	607056
Analysis_Date	3/16/95
Instrument	JSM-840

Mag	Fields	particles
200	1.098	199
400	0.971	200
800	0.477	100

Classes	#	Number %	Wt %	Ave. size
C-rich	97	65.04	1.28	0.4
Si-rich	91	14.58	16.37	1.2
Ca-rich	7	0.51	0.77	2.4
Fe-rich	12	1.59	2.52	1.5
Mixed clay	292	18.28	79.05	2.7
Totals	499	100.00	100.00	1.0

Table A

Number Distribution by Average Diameter (microns)

		0.2 - 2.5	2.5 - 5.0	5.0 - 10.0	10.0 - 15.0	15.0 - 20.0	20.0 - 25.0	25.0 - 30.0
Classes	Number							
C-rich	97	94	1	2	0	0	0	0
Si-rich	91	45	24	21	1	0	0	0
Ca-rich	7	3	2	2	0	0	0	0
Fe-rich	12	6	3	3	0	0	0	0
Mixed clay	292	92	112	83	5	0	0	0
Totals	499	240	142	111	6	0	0	0

Table B

Size Distribution by Average Diameter (microns)

		0.2 - 2.5	2.5 - 5.0	5.0 - 10.0	10.0 - 15.0	15.0 - 20.0	20.0 - 25.0	25.0 - 30.0
Classes	Number %							
C-rich	65.0	99.8	0.1	0.1	0.0	0.0	0.0	0.0
Si-rich	14.6	89.4	7.5	3.0	0.1	0.0	0.0	0.0
Ca-rich	0.5	55.1	36.8	8.1	0.0	0.0	0.0	0.0
Fe-rich	1.6	78.2	17.9	3.9	0.0	0.0	0.0	0.0
Mixed clay	18.3	58.6	31.3	9.5	0.6	0.0	0.0	0.0
Totals	100.0	90.2	7.4	2.3	0.1	0.0	0.0	0.0

Table C

Client_Name	MOA-DHHS
Client_Number	PM10#83
Project_Number	ESH503033
Sample_Number	607056
Analysis_Date	3/16/95
Instrument	JSM-840

Mass Distribution by Average Diameter (microns)

		0.2 -	2.5 -	5.0 -	10.0 -	15.0 -	20.0 -	25.0 -
Classes	Mass %	2.5	5.0	10.0	15.0	20.0	25.0	30.0
C-rich	1.3	32.7	24.2	43.0	0.0	0.0	0.0	0.0
Si-rich	16.4	8.0	23.1	53.6	15.4	0.0	0.0	0.0
Ca-rich	0.8	7.3	41.8	50.9	0.0	0.0	0.0	0.0
Fe-rich	2.5	11.7	47.5	40.8	0.0	0.0	0.0	0.0
Mixed clay	79.1	5.6	27.3	52.3	14.9	0.0	0.0	0.0
Totals	100.0	6.5	27.2	52.1	14.3	0.0	0.0	0.0

Table D

Aerodynamic Mass Distribution by Aerodynamic Diameter (microns)

		0.2 -	2.5 -	5.0 -	10.0 -	15.0 -	20.0 -	25.0 -
Classes	Mass %	2.5	5.0	10.0	15.0	20.0	25.0	30.0
C-rich	1.3	32.7	24.2	43.0	0.0	0.0	0.0	0.0
Si-rich	16.4	3.8	13.4	52.5	14.8	15.4	0.0	0.0
Ca-rich	0.8	7.3	41.8	50.9	0.0	0.0	0.0	0.0
Fe-rich	2.5	2.6	19.0	78.4	0.0	0.0	0.0	0.0
Mixed clay	79.1	2.1	13.0	44.0	29.8	11.1	0.0	0.0
Totals	100.0	2.8	13.6	46.3	26.0	11.3	0.0	0.0

Table E

Average Composition

Classes	#	C	O	NA	MG	AL	SI	P	S	CL	K	CA	TI	CR	MN	FE	NI	CU	ZN	AS	PB
C-rich	97	91	1	0	0	0	4	0	1	0	0	0	0	0	0	0	0	0	0	0	0
Si-rich	91	38	6	0	0	0	54	0	1	0	0	1	0	0	0	0	0	0	0	0	0
Ca-rich	7	30	8	0	0	3	11	4	11	0	3	25	0	0	0	3	0	0	1	0	0
Fe-rich	12	28	6	0	0	2	8	0	1	0	1	1	0	0	1	53	0	0	0	0	0
Mixed clay	292	15	6	1	1	15	46	0	0	0	3	4	0	0	0	8	0	0	0	0	0
Totals	499	68	3	0	0	3	19	0	1	0	1	1	0	0	0	2	0	0	0	0	0

Table F

Client_Name	MOA-DHHS
Client_Number	PM10#128
Project_Number	ESH503033
Sample_Number	607057
Analysis_Date	3/15/95
Instrument	JSM-840

Mag	Fields	particles
200	2.703	200
400	1.572	199
800	0.752	100

Classes	#	Number %	Wt %	Ave. size
C-rich	104	62.07	5.01	0.4
Si-rich	48	8.44	7.54	0.9
Ca-rich	4	0.91	0.62	0.8
Fe-rich	8	0.67	0.79	1.6
Mixed clay	333	26.34	86.03	1.9
Misc	2	1.57	0.01	0.4
Totals	499	100.00	100.00	0.9

Table A

Number Distribution by Average Diameter (microns)

		0.2 -	2.5 -	5.0 -	10.0 -	15.0 -	20.0 -	25.0 -
Classes	Number	2.5	5.0	10.0	15.0	20.0	25.0	30.0
C-rich	104	92	3	9	0	0	0	0
Si-rich	48	27	8	13	0	0	0	0
Ca-rich	4	2	0	2	0	0	0	0
Fe-rich	8	7	1	0	0	0	0	0
Mixed clay	333	115	114	102	2	0	0	0
Misc	2	2	0	0	0	0	0	0
Totals	499	245	126	126	2	0	0	0

Table B

Size Distribution by Average Diameter (microns)

		0.2 -	2.5 -	5.0 -	10.0 -	15.0 -	20.0 -	25.0 -
Classes	Number %	2.5	5.0	10.0	15.0	20.0	25.0	30.0
C-rich	62.1	99.7	0.1	0.2	0.0	0.0	0.0	0.0
Si-rich	8.4	95.6	2.2	2.1	0.0	0.0	0.0	0.0
Ca-rich	0.9	97.0	0.0	3.0	0.0	0.0	0.0	0.0
Fe-rich	0.7	98.0	2.0	0.0	0.0	0.0	0.0	0.0
Mixed clay	26.3	72.5	22.1	5.3	0.1	0.0	0.0	0.0
Misc	1.6	100.0	0.0	0.0	0.0	0.0	0.0	0.0
Totals	100.0	92.2	6.1	1.7	0.0	0.0	0.0	0.0

Table C

Client_Name MOA-DHHS
Client_Number PM10#128
Project_Number ESH503033
Sample_Number 607057
Analysis_Date 3/15795
Instrument JSM-840

Mass Distribution by Average Diameter (microns)

		0.2 -	2.5 -	5.0 -	10.0 -	15.0 -	20.0 -	25.0 -
Classes	Mass %	2.5	5.0	10.0	15.0	20.0	25.0	30.0
C-rich	5.0	15.4	3.7	80.8	0.0	0.0	0.0	0.0
Si-rich	7.5	14.6	14.6	70.7	0.0	0.0	0.0	0.0
Ca-rich	0.6	22.0	0.0	78.0	0.0	0.0	0.0	0.0
Fe-rich	0.8	72.6	27.4	0.0	0.0	0.0	0.0	0.0
Mixed clay	86.0	7.9	34.3	51.4	6.4	0.0	0.0	0.0
Misc	0.0	100.0	0.0	0.0	0.0	0.0	0.0	0.0
Totals	100.0	9.4	31.0	54.1	5.5	0.0	0.0	0.0

Table D

Aerodynamic Mass Distribution by Aerodynamic Diameter (microns)

		0.2 -	2.5 -	5.0 -	10.0 -	15.0 -	20.0 -	25.0 -
Classes	Mass %	2.5	5.0	10.0	15.0	20.0	25.0	30.0
C-rich	5.0	14.3	3.7	36.8	45.1	0.0	0.0	0.0
Si-rich	7.5	8.9	8.9	51.8	30.5	0.0	0.0	0.0
Ca-rich	0.6	1.2	20.8	78.0	0.0	0.0	0.0	0.0
Fe-rich	0.8	19.8	52.8	27.4	0.0	0.0	0.0	0.0
Mixed clay	86.0	3.0	19.9	52.6	18.1	6.4	0.0	0.0
Misc	0.0	100.0	0.0	0.0	0.0	0.0	0.0	0.0
Totals	100.0	4.1	18.5	51.7	20.1	5.5	0.0	0.0

Table E

Average Composition

Classes	#	C	O	NA	MG	AL	SI	P	S	CL	K	CA	TI	CR	MN	FE	NI	CU	ZN	AS	PB
C-rich	104	97	0	0	0	1	0	0	1	0	0	0	0	0	0	0	0	0	0	0	0
Si-rich	48	27	6	0	0	0	65	0	0	0	0	1	0	0	0	0	0	0	0	0	0
Ca-rich	4	19	6	0	0	0	2	0	26	0	0	46	0	0	0	0	0	0	0	0	0
Fe-rich	8	2	4	0	1	1	9	0	0	0	0	0	4	0	0	80	0	0	0	0	0
Mixed clay	333	9	7	0	2	14	53	0	0	0	1	6	0	0	0	7	0	0	0	0	0
Misc	2	58	0	0	0	0	0	0	0	19	0	0	24	0	0	0	0	0	0	0	0
Totals	499	66	3	0	1	4	20	0	1	0	0	2	0	0	0	2	0	0	0	0	0

Table F

Client_Name	MOA-DHHS
Client_Number	PM10#131
Project_Number	ESH503033
Sample_Number	607058
Analysis_Date	3/15/95
Instrument	JSM-840

Mag	Fields	particles
200	0.954	200
400	0.788	200
800	0.701	99

Classes	#	Number %	Wt %	Ave. size
C-rich	93	52.03	0.93	0.5
Si-rich	74	13.93	11.57	1.3
Ca-rich	11	1.14	3.75	2.3
Fe-rich	10	1.34	0.80	1.5
Mixed clay	310	31.53	80.03	2.5
Misc	1	0.03	2.93	13.3
Totals	499	100.00	100.00	1.3

Table A

Number Distribution by Average Diameter (microns)

		0.2 -	2.5 -	5.0 -	10.0 -	15.0 -	20.0 -	25.0 -
Classes	Number	2.5	5.0	10.0	15.0	20.0	25.0	30.0
C-rich	93	90	1	2	0	0	0	0
Si-rich	74	36	18	20	0	0	0	0
Ca-rich	11	6	2	2	1	0	0	0
Fe-rich	10	9	0	1	0	0	0	0
Mixed clay	310	102	100	103	5	0	0	0
Misc	1	0	0	0	1	0	0	0
Totals	499	243	121	128	7	0	0	0

Table B

Size Distribution by Average Diameter (microns)

		0.2 -	2.5 -	5.0 -	10.0 -	15.0 -	20.0 -	25.0 -
Classes	Number %	2.5	5.0	10.0	15.0	20.0	25.0	30.0
C-rich	52.0	99.6	0.3	0.1	0.0	0.0	0.0	0.0
Si-rich	13.9	85.2	10.5	4.3	0.0	0.0	0.0	0.0
Ca-rich	1.1	76.7	15.4	5.3	2.6	0.0	0.0	0.0
Fe-rich	1.3	97.8	0.0	2.2	0.0	0.0	0.0	0.0
Mixed clay	31.5	63.3	26.4	9.8	0.5	0.0	0.0	0.0
Misc	0.0	0.0	0.0	0.0	100.0	0.0	0.0	0.0
Totals	100.0	85.8	10.1	3.9	0.2	0.0	0.0	0.0

Table C

Client_Name	MOA-DHHS
Client_Number	PM10#131
Project_Number	ESH503033
Sample_Number	607058
Analysis_Date	3/15/95
Instrument	JSM-840

Mass Distribution by Average Diameter (microns)

		0.2 -	2.5 -	5.0 -	10.0 -	15.0 -	20.0 -	25.0 -
Classes	Mass %	2.5	5.0	10.0	15.0	20.0	25.0	30.0
C-rich	0.9	39.2	12.9	47.9	0.0	0.0	0.0	0.0
Si-rich	11.6	6.2	23.9	69.9	0.0	0.0	0.0	0.0
Ca-rich	3.7	5.1	11.7	17.8	65.4	0.0	0.0	0.0
Fe-rich	0.8	30.2	0.0	69.8	0.0	0.0	0.0	0.0
Mixed clay	80.0	5.8	21.9	59.8	12.5	0.0	0.0	0.0
Misc	2.9	0.0	0.0	0.0	100.0	0.0	0.0	0.0
Totals	100.0	6.2	20.8	57.6	15.4	0.0	0.0	0.0

Table D

Aerodynamic Mass Distribution by Aerodynamic Diameter (microns)

		0.2 -	2.5 -	5.0 -	10.0 -	15.0 -	20.0 -	25.0 -
Classes	Mass %	2.5	5.0	10.0	15.0	20.0	25.0	30.0
C-rich	0.9	33.9	18.2	47.9	0.0	0.0	0.0	0.0
Si-rich	11.6	3.2	14.0	44.0	38.9	0.0	0.0	0.0
Ca-rich	3.7	2.2	11.2	21.2	0.0	65.4	0.0	0.0
Fe-rich	0.8	18.9	11.3	0.0	69.8	0.0	0.0	0.0
Mixed clay	80.0	1.9	13.3	39.7	34.3	10.8	0.0	0.0
Misc	2.9	0.0	0.0	0.0	0.0	100.0	0.0	0.0
Totals	100.0	2.4	12.9	38.1	32.5	14.1	0.0	0.0

Table E

Average Composition

Classes	#	C	O	NA	MG	AL	SI	P	S	CL	K	CA	TI	CR	MN	FE	NI	CU	ZN	AS	PB
C-rich	93	88	2	0	0	1	5	0	1	0	0	1	0	0	0	0	0	0	0	0	0
Si-rich	74	34	7	0	0	0	56	0	0	0	0	1	0	0	0	1	0	0	0	0	0
Ca-rich	11	12	5	0	0	2	9	10	9	0	0	47	3	0	0	1	0	0	0	0	0
Fe-rich	10	19	6	0	0	3	10	0	3	1	0	2	0	0	0	54	0	1	0	0	0
Mixed clay	310	15	7	1	1	14	46	0	0	0	2	5	1	0	0	7	0	0	0	0	0
Misc	1	65	0	5	0	0	9	0	0	14	7	0	0	0	0	0	0	0	0	0	0
Totals	499	56	4	0	0	5	25	0	1	0	1	3	1	0	0	3	0	0	0	0	0

Table F

Client_Name	MOA-DHHS
Client_Number	PM10#198
Project_Number	ESH503033
Sample_Number	607059
Analysis_Date	3/14/95
Instrument	JSM-840

Mag	Fields	particles
200	3.211	199
400	1.477	200
800	1.004	100

Classes	#	Number %	Wt %	Ave. size
C-rich	109	57.22	3.24	0.5
Si-rich	82	12.97	17.10	1.2
Ca-rich	14	1.18	2.44	2.1
Fe-rich	7	0.75	1.16	1.9
Mixed clay	285	27.03	76.01	1.9
Misc	2	0.85	0.05	0.5
Totals	499	100.00	100.00	1.0

Table A

Number Distribution by Average Diameter (microns)

		0.2 - 2.5	2.5 - 5.0	5.0 - 10.0	10.0 - 15.0	15.0 - 20.0	20.0 - 25.0	25.0 - 30.0
Classes	Number							
C-rich	109	98	6	5	0	0	0	0
Si-rich	82	36	20	25	1	0	0	0
Ca-rich	14	7	3	4	0	0	0	0
Fe-rich	7	6	1	0	0	0	0	0
Mixed clay	285	107	93	81	4	0	0	0
Misc	2	2	0	0	0	0	0	0
Totals	499	256	123	115	5	0	0	0

Table B

Size Distribution by Average Diameter (microns)

		0.2 - 2.5	2.5 - 5.0	5.0 - 10.0	10.0 - 15.0	15.0 - 20.0	20.0 - 25.0	25.0 - 30.0
Classes	Number %							
C-rich	57.2	99.0	0.9	0.1	0.0	0.0	0.0	0.0
Si-rich	13.0	89.9	7.2	2.7	0.1	0.0	0.0	0.0
Ca-rich	1.2	73.1	22.1	4.8	0.0	0.0	0.0	0.0
Fe-rich	0.8	98.1	1.9	0.0	0.0	0.0	0.0	0.0
Mixed clay	27.0	77.8	17.8	4.2	0.2	0.0	0.0	0.0
Misc	0.8	100.0	0.0	0.0	0.0	0.0	0.0	0.0
Totals	100.0	91.8	6.5	1.6	0.1	0.0	0.0	0.0

Table C

Client_Name	MOA-DHHS
Client_Number	PM10#198
Project_Number	ESH503033
Sample_Number	607059
Analysis_Date	3/14/95
Instrument	JSM-840

Mass Distribution by Average Diameter (microns)

		0.2 -	2.5 -	5.0 -	10.0 -	15.0 -	20.0 -	25.0 -
Classes	Mass %	2.5	5.0	10.0	15.0	20.0	25.0	30.0
C-rich	3.2	30.6	34.1	35.3	0.0	0.0	0.0	0.0
Si-rich	17.1	7.2	21.3	59.7	11.8	0.0	0.0	0.0
Ca-rich	2.4	14.8	38.8	46.4	0.0	0.0	0.0	0.0
Fe-rich	1.2	79.8	20.2	0.0	0.0	0.0	0.0	0.0
Mixed clay	76.0	10.1	27.0	50.0	12.9	0.0	0.0	0.0
Misc	0.1	100.0	0.0	0.0	0.0	0.0	0.0	0.0
Totals	100.0	11.3	26.5	50.5	11.8	0.0	0.0	0.0

Table D

Aerodynamic Mass Distribution by Aerodynamic Diameter (microns)

		0.2 -	2.5 -	5.0 -	10.0 -	15.0 -	20.0 -	25.0 -
Classes	Mass %	2.5	5.0	10.0	15.0	20.0	25.0	30.0
C-rich	3.2	27.1	36.6	36.3	0.0	0.0	0.0	0.0
Si-rich	17.1	4.5	14.3	42.1	27.2	11.8	0.0	0.0
Ca-rich	2.4	9.2	15.2	75.6	0.0	0.0	0.0	0.0
Fe-rich	1.2	2.8	77.0	20.2	0.0	0.0	0.0	0.0
Mixed clay	76.0	3.8	18.8	40.1	26.2	11.1	0.0	0.0
Misc	0.1	100.0	0.0	0.0	0.0	0.0	0.0	0.0
Totals	100.0	4.9	19.2	41.0	24.6	10.4	0.0	0.0

Table E

Average Composition

Classes	#	C	O	NA	MG	AL	SI	P	S	CL	K	CA	TI	CR	MN	FE	NI	CU	ZN	AS	PB
C-rich	109	98	0	0	0	0	1	0	0	0	0	0	0	0	0	0	0	0	0	0	0
Si-rich	82	23	5	0	0	0	69	0	0	1	0	0	0	0	0	2	0	0	0	0	0
Ca-rich	14	24	4	0	2	2	6	0	7	0	0	52	3	0	0	0	0	0	0	0	0
Fe-rich	7	5	4	0	0	2	4	0	0	2	0	2	1	0	0	79	0	0	0	0	0
Mixed clay	285	14	6	1	1	17	48	0	0	0	1	5	0	0	0	7	0	0	0	0	0
Misc	2	64	0	0	0	0	0	0	0	15	0	0	14	0	0	0	0	7	0	0	0
Totals	499	64	2	0	0	5	23	0	0	0	0	2	0	0	0	3	0	0	0	0	0

Table F

Client_Name	MOA-DHHS
Client_Number	PM10#305
Project_Number	ESH503033
Sample_Number	607060
Analysis_Date	3/15/95
Instrument	JSM-840

Mag	Fields	particles
200	1.855	199
400	1.011	200
800	0.475	99

Classes	#	Number %	Wt %	Ave. size
C-rich	82	54.15	1.28	0.4
Si-rich	32	9.21	4.66	0.8
Ca-rich	6	0.40	0.99	2.1
Fe-rich	9	0.60	2.15	2.2
Mixed clay	367	34.84	90.75	1.6
Misc	2	0.81	0.17	0.8
Totals	498	100.00	100.00	0.9

Table A

Number Distribution by Average Diameter (microns)

		0.2 -	2.5 -	5.0 -	10.0 -	15.0 -	20.0 -	25.0 -
Classes	Number	2.5	5.0	10.0	15.0	20.0	25.0	30.0
C-rich	82	75	2	5	0	0	0	0
Si-rich	32	22	4	6	0	0	0	0
Ca-rich	6	3	1	2	0	0	0	0
Fe-rich	9	5	1	3	0	0	0	0
Mixed clay	367	155	105	104	3	0	0	0
Misc	2	1	1	0	0	0	0	0
Totals	498	261	114	120	3	0	0	0

Table B

Size Distribution by Average Diameter (microns)

		0.2 -	2.5 -	5.0 -	10.0 -	15.0 -	20.0 -	25.0 -
Classes	Number %	2.5	5.0	10.0	15.0	20.0	25.0	30.0
C-rich	54.1	99.8	0.0	0.1	0.0	0.0	0.0	0.0
Si-rich	9.2	98.6	0.6	0.8	0.0	0.0	0.0	0.0
Ca-rich	0.4	70.2	23.4	6.4	0.0	0.0	0.0	0.0
Fe-rich	0.6	78.0	15.6	6.4	0.0	0.0	0.0	0.0
Mixed clay	34.8	83.9	12.2	3.8	0.1	0.0	0.0	0.0
Misc	0.8	98.4	1.6	0.0	0.0	0.0	0.0	0.0
Totals	100.0	93.9	4.5	1.5	0.0	0.0	0.0	0.0

Table C

Client_Name	MOA-DHHS
Client_Number	PM10#305
Project_Number	ESH503033
Sample_Number	607060
Analysis_Date	3/15/95
Instrument	JSM-840

Mass Distribution by Average Diameter (microns)

		0.2 -	2.5 -	5.0 -	10.0 -	15.0 -	20.0 -	25.0 -
Classes	Mass %	2.5	5.0	10.0	15.0	20.0	25.0	30.0
C-rich	1.3	27.9	9.3	62.9	0.0	0.0	0.0	0.0
Si-rich	4.7	13.0	11.4	75.6	0.0	0.0	0.0	0.0
Ca-rich	1.0	10.5	21.2	68.3	0.0	0.0	0.0	0.0
Fe-rich	2.1	21.7	21.4	56.9	0.0	0.0	0.0	0.0
Mixed clay	90.8	10.6	25.7	55.6	8.2	0.0	0.0	0.0
Misc	0.2	10.6	89.4	0.0	0.0	0.0	0.0	0.0
Totals	100.0	11.2	24.8	56.6	7.4	0.0	0.0	0.0

Table D

Aerodynamic Mass Distribution by Aerodynamic Diameter (microns)

		0.2 -	2.5 -	5.0 -	10.0 -	15.0 -	20.0 -	25.0 -
Classes	Mass %	2.5	5.0	10.0	15.0	20.0	25.0	30.0
C-rich	1.3	27.9	9.3	62.9	0.0	0.0	0.0	0.0
Si-rich	4.7	9.8	3.2	49.8	37.2	0.0	0.0	0.0
Ca-rich	1.0	10.5	21.2	68.3	0.0	0.0	0.0	0.0
Fe-rich	2.1	6.0	15.7	56.1	22.2	0.0	0.0	0.0
Mixed clay	90.8	3.8	19.4	38.4	32.7	5.8	0.0	0.0
Misc	0.2	10.6	0.0	89.4	0.0	0.0	0.0	0.0
Totals	100.0	4.5	18.4	40.0	31.9	5.3	0.0	0.0

Table E

Average Composition

Classes	#	C	O	NA	MG	AL	SI	P	S	CL	K	CA	TI	CR	MN	FE	NI	CU	ZN	AS	PB
C-rich	82	94	0	0	0	0	2	0	2	0	1	0	0	0	0	0	0	0	0	0	0
Si-rich	32	32	4	0	0	0	55	0	2	1	0	2	1	0	0	3	0	0	0	0	0
Ca-rich	6	28	6	2	0	2	15	0	20	0	2	25	0	0	0	0	0	0	0	0	0
Fe-rich	9	5	2	0	0	1	7	0	34	0	1	1	1	0	0	48	0	0	0	0	0
Mixed clay	367	14	7	0	1	14	48	0	0	0	1	9	0	0	0	5	0	0	0	0	0
Misc	2	67	0	0	0	1	17	0	0	0	0	0	0	0	15	0	0	0	0	0	0
Totals	498	59	3	0	1	5	23	0	2	0	1	4	0	0	0	2	0	0	0	0	0

Table F

Reprinted from
American Laboratory
November 1989

By B.C. Henderson, I.M. Stewart, and G.S Casuccio

Rapid acquisition/storage of electron microscope images

THE SCIENCE OF microscopy, historically limited to optical or light microscopy, can provide a tremendous amount of information on specimens too small to be examined with the unaided eye. The optical microscope has been, and will continue to be, a powerful analytical tool for providing size information about the morphology of microscopic features. The optical microscope's practical resolution, however, is ultimately limited by the wavelengths associated with light of the visible spectrum. When features of interest begin to occur in micron and sub-micron size ranges, detailed resolution is lost. Since complete characterization of materials is often dependent on an understanding of microstructure, the analytical world needed a tool capable of providing information, not only on morphology, but also on composition and at sizes well beyond capabilities of the light microscope.

The requirement for additional resolution of microscopic features led to experimentation during the first half of this century using accelerated electrons to strike the specimen and form an image. It was soon discovered that a fine beam of electrons provided better image resolution, a wider range of magnifications for viewing, and a tremendous increase in depth-of-field when compared with images formed using visible light. In addition to enhanced imaging capabilities, the impinging electron beam was also found to generate many other signals, often yielding a wealth of information about the specimen.

Experimentation with electrons ultimately resulted in development of the transmission electron microscope (TEM) and the scanning electron microscope (SEM), two of the most important analytical instruments in use today. In the SEM and scanning TEM (or STEM), a minutely focused electron beam is rastered over the specimen. As the beam strikes the sample, various signals are generated, which include secondary, backscattered, and Auger electrons, characteristic x-rays, photons, and cathodoluminescence. These signals may be collected in synchronization with the beam position to provide highly detailed information on a point-by-point basis.

The secondary electron signal yields an image of the specimen with three-dimensional perspective, high depth-of-field, and the appearance of overhead illumination. Backscattered electron images are often used for discriminating between phases containing elements of different atomic number. Specific information about elemental composition can be acquired through the collection and processing of x-rays emitted as a result of the electron beam striking the sample. X-rays of characteristic energy and wavelength are emitted from atoms of the different elements present in the material of the sample and may be detected and sorted to identify elemental composition.

The science of electron microscopy has undergone significant advancement since the advent of the SEM over twenty years ago. In the past, manipulation of SEM and STEM controls for analytical purposes was performed in a manual fashion. Typically, specimens containing particle populations would be characterized by having a scientist search the sample in the SEM for particles having a size, morphology, and/or chemistry of interest. Elemental spectra and photomicrographs would be collected, one at a time, to describe the individual features present.

When employing any of the microscopy disciplines, such manual examination of multiple fine particles or features is very time consuming and tedious. The data generated from such analyses are often considered to be only statistically qualitative because of the relatively small number of features or particles that can be characterized in a reasonable period of time. In addition, in attempting to adequately characterize an overall structure by microscopical methods, there is a natural tendency on the part of the observer to select unusual or aesthetically pleasing features rather than the typical, and often less interesting. Thus operator bias is often a problem when extended periods of time are required to characterize a great number of a specimen's components.

Automated or computer control of the SEM has allowed scientists to bridge the gap between statistically qualitative analyses of particle samples and quantitative analyses descriptive of an entire population of features. Computer-controlled SEM (CCSEM) is accomplished by the controlled manipulation of the electron beam that is rastering over the sample's surface. Based on signals generated as the impinging electrons strike the sample, features are identified, measured, and x-ray information obtained automatically. Data from the individual particle or fea-

The authors are with the RJ Lee Group, Monroeville, Pennsylvania, U.S.A. *The authors would like to acknowledge the assistance of Ray Callihan for producing the figures in this article.*

ture are ultimately sorted and summarized by the computer to describe the entire specimen based on various factors. Calculations can be performed detailing a specimen's features by parameters such as number percent, weight percent, area percent, aspect ratio, and elemental composition. Therefore, size and composition correlations can be formulated to specifically identify and label specimen constituents. This technology has been described in greater detail elsewhere.[1]

The advantages associated with such automated particle analysis quickly became apparent to the scientist, as did its limitations. More often than not, microscopy examinations take the analyst into unknown territory. Frequently, a feature's morphology and surface texture prove to be crucial factors in its proper characterization. CCSEM analyses were essentially lacking information that only the photomicrograph of a manual investigation could provide. In short, the limiting factor to automated analyses was that images from individual features of interest were lost when the scientist relied on computer control of the instrumentation.

This concern has been addressed by the enhancement of CCSEM (by RJ Lee Group, Monroeville, Pennsylvania) to permit the collection of an image of each particle or feature examined during the automated analysis in addition to the aforementioned parameters. The concept of performing a CCSEM analysis while acquiring and archiving the image of a feature is called MicroImaging. MicroImaging, or the acquisition and storage of individual, high-resolution images, has evolved from an existing analytical method pioneered by United States Steel Research (Monroeville, Pennsylvania) and Tracor Northern (Middleton, Wisconsin).[2-4] Through the use of software, it is possible to dynamically alter the position and apparent magnification of the digitally rastered electron beam in order to acquire images and direct these to magnetic or optical media for storage.[5]

MicroImaging with CCSEM is made possible by interfacing a microcomputer with a conventional SEM (or STEM) for the purpose of controlling the energy dispersive spectrometer, an automated stage, and a digital scan generator. In addition to collecting size, shape, position, and spectral data for each individual particle, MicroImaging enables high-resolution images of the analyzed features to be acquired and stored. Images of each particle analyzed may be saved, or, alternatively, algorithms may be applied during the data acquisition process to select images based on x-ray, size, or shape criteria.

In order to accomplish MicroImaging, three additions have been made to existing automated particle analysis technology. The first is the use of an automated stage. By defining a local coordinate system, it is possible to record the position of each feature analyzed. In the event that a reexamination of that feature is required, it is possible, by reinitializing the stage with respect to index marks on the sample, to drive the stage to the specific coordinates of the feature of interest.

The second addition is the interfacing of the digital scan generator to control both raster position and size. It is thus possible, by software control, to alter both magnification and beam position to enable microimages of selected features to be acquired.

Finally, in order to exploit the full capabilities of the system, a high-speed data link between the SEM and energy dispersive spectroscopy (EDS) system, as well as a computer workstation, was developed (RJ Lee Group) to allow the transmission of images during collection of an x-ray spectrum for the particle being analyzed.

The images and data collected during the sample examination are stored on magnetic or optical media which are removable. Examples are Bernoulli disks or optical WORM (Write Once Read Many) devices. These may then be transferred to off-line computer workstations where the data may be retrieved, examined, and interrogated. *Figure 1* illustrates the architecture associated with the MicroImaging system.

An important feature of the MicroImaging system (RJ Lee Group) is the data manipulation that can be performed off-line. Data management programs have been developed which enable the researcher to display the particle chemistry in a variety of ways:

1. A ternary plotting routine permits display of particle compositions within a ternary composition diagram, the vertices of which may be assigned by the observer while the use of color permits a fourth "dimension" to be added, such as the size variations of particles or, perhaps, the presence or absence of additional elements. A mouse-driven cursor allows selection within the ternary plot of individual particles, the complete chemistry and stored image of which may then be retrieved and displayed. *Figure 2* presents a ternary diagram based on the analysis of inclusions in a stainless steel sample.

2. Application of selected mineral composition algorithms permits a modal analysis to be performed in which the computer assigns a mineral composition to each particle and presents an overall mineral composition of the bulk material.

3. Sizing algorithms enable rapid size distribution determinations and their correlation with shape and/or chemical composition factors. Such investigations frequently give preliminary indications of the number of possible components present within the sample.

4. Image files of standards may be generated and combined with their elemental composition to produce electronic encyclopedias of various standards. A pollen Atlas has already been generated and work is in progress on various Atlases of minerals and other particulate matter. *Figure 3* is a digitized image from the electronic pollen Atlas.

Because MicroImaging data are readily accessible at an off-line workstation, researchers are no longer limited in their investigations by the availability of time on a re-

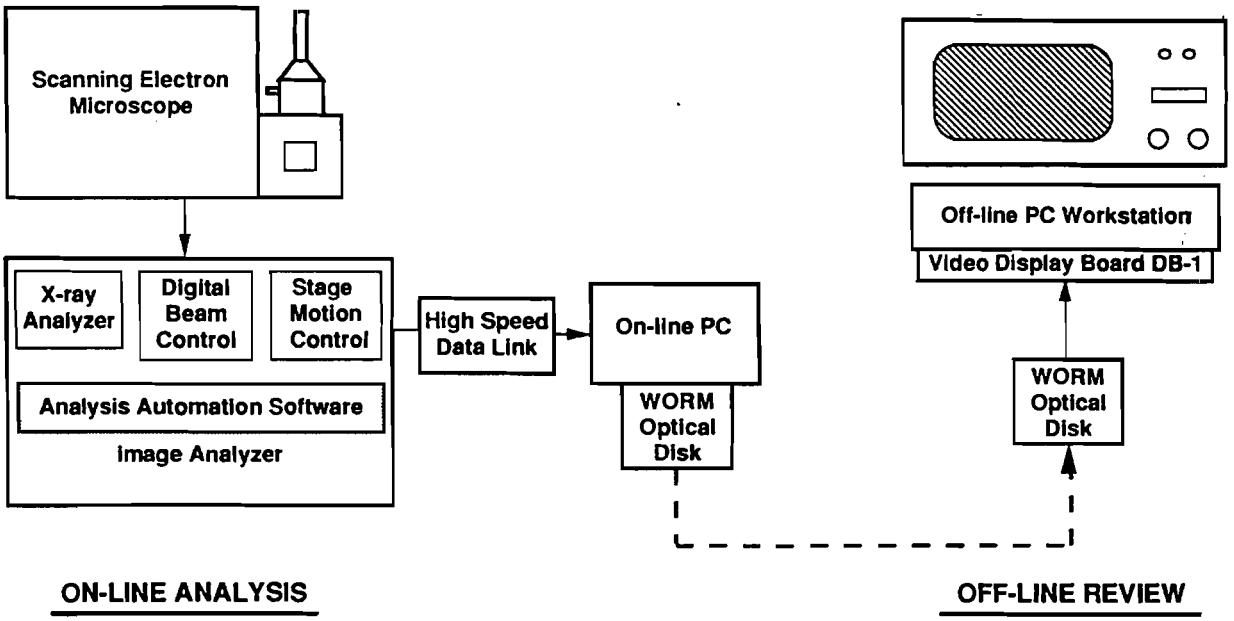

Figure 1 *Schematic illustrating the architecture associated with on-line and off-line components of the MicroImaging workstation.*

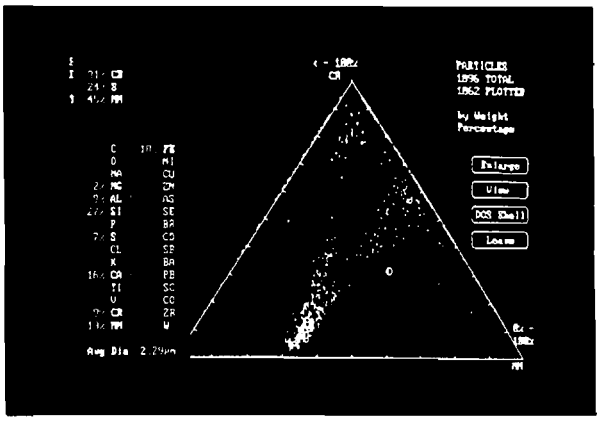

Figure 2 *Ternary diagram of Mn, S, and Cr inclusions observed in a stainless steel sample. The ring cursor enables the operator to isolate any individual inclusion. The table at the left of the diagram displays the full elemental analysis and the size of the inclusion.*

search microscope. One microscope can generate enough data to support numerous workstations, and the extent to which the data may be manipulated and interrogated is limited, for the most part, only by the ingenuity and persistence of the investigator. *Figure 4* depicts the off-line MicroImaging workstation.

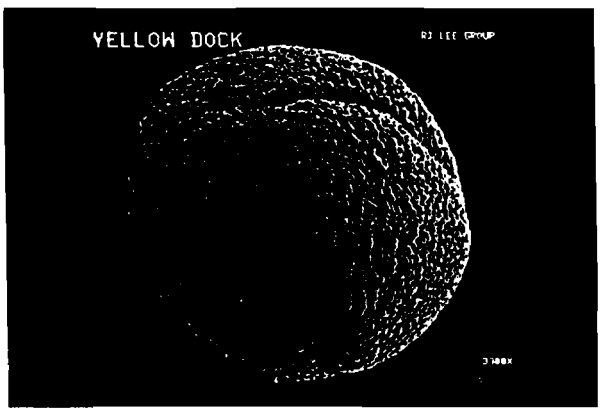

Figure 3 *Digitized secondary electron image of a pollen particle acquired with a pixel resolution of 512 × 512 using MicroImaging technology. This image is taken from an "electronic encyclopedia" of pollens which is being developed at RJ Lee Group, Inc.*

Summary

MicroImaging technology as applied to the SEM may be described as the rapid acquisition and digital storage of images of each feature examined as well as data on particle size and elemental composition (classical CCSEM). In essence, MicroImaging links aspects of manual and automated specimen analyses. With this method, it is possible to describe a sample more efficiently than with manual methods alone, and more cost effectively than with on-line interpretation of data.[6,7] In the future, the data collection, storage, retrieval, and manipulation technologies that collectively make up MicroImaging should

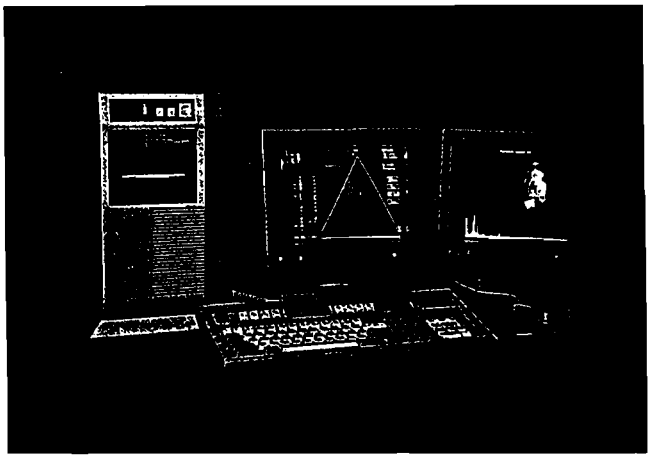

Figure 4 *MicroImaging off-line workstation consisting of a tower-design PC with an internally mounted WORM drive, graphics monitors, keyboard, and mouse.*

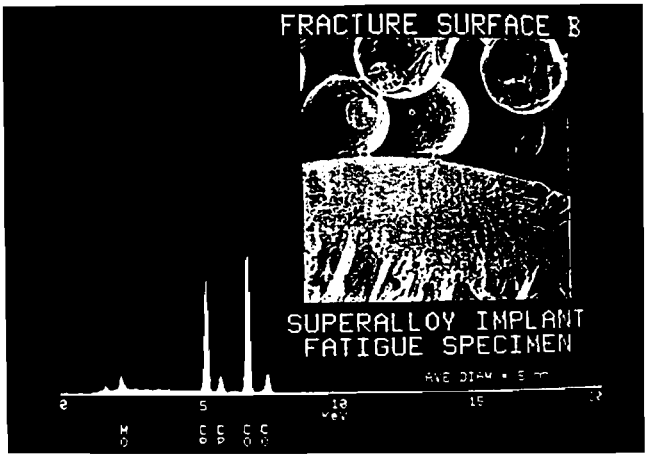

Figure 5 *A digital image displayed from an off-line MicroImaging workstation showing a fracture surface associated with a fatigue test specimen composed of a cast Co-Cr-Mo alloy.*

make possible the use of advanced data interrogation schemes such as artificial intelligence and fractal geometry in the analysis of particulate samples, composite materials, and metal and ceramic microstructures. *Figure 5* presents a digital image of a metal alloy specimen.

MicroImaging techniques are also being applied to conventional TEM images captured through use of a high-resolution television system. Here the potential for the application of MicroImaging techniques in the biomedical field, particularly to stereological studies performed on serial sections, promises to be an exciting one.

References

1. LEE, R.J. and FISHER, R.M., "Quantitative characterization of particulates by scanning and high voltage microscopy," National Bureau of Standards, Special Publication 533, *Characterization of Particles*, 1980, p. 63.
2. LEE, R.J. et al., "Quantitative metallography by computer-controlled scanning electron microscopy," *Journals of Metals* (U.S. Steel Corporation, Research Laboratory, Monroeville, PA), 20-25 (March 1981).
3. FISHER, R.M., LEE, R.J., and MC CARTHY, J.J., "Applications of computers in electron microscopy," *Ultramicroscopy 8*, 351-360 (1982).
4. LEE, R.J. and WALKER, J.S., "Automation in microscopy," presented at the *Society of Photographic Scientists and Engineers* (Newport, RI, December 1985).
5. MERSHON, W.J. et al., "Application of MicroImaging to computer-controlled scanning electron microscopy," presented at *EMSA* (1988).
6. CASUCCIO, G.S. et al., "The use of CCSEM and MicroImaging to study source/receptor relationships," *APCA Specialty Conference* (San Francisco, CA, 1988).
7. SCHWOEBLE, A.J. et al., "Computer-controlled SEM and MicroImaging of fine particles," *Jour. of Metals* (Aug. 1988).

Reprinted from APCA JOURNAL, Vol. 33, No. 10, October 1983

The Use of Computer Controlled Scanning Electron Microscopy in Environmental Studies

Gary S. Casuccio and Philip B. Janocko
Energy Technology Consultants/Atmospheric Research Organization, Inc.
Murrysville, Pennsylvania
Richard J. Lee and James F. Kelly
United States Steel Research
Monroeville, Pennsylvania
Stuart L. Dattner and J. Scott Mgebroff
Texas Air Control Board
Austin, Texas

The microscope has long been used to identify the chemical and morphological characteristics of features too small to be detected with the naked eye. The ability to analyze individual microscopic features provides a resolution of sample constituents and their associations unobtainable by most gross or bulk analysis methods. Because of this increased resolution, both light (optical) and electron microscopy have often been employed in the analysis of particulate matter. However, manual microscopic analysis is both tedious and time consuming. Therefore, the results obtained from manual microscopic analysis have usually been only qualitative because of the relatively small number of particles characterized. A quantitative analysis requires reproducible sizing and identification of individual particles in numbers sufficient to satisfy statistical counting requirements. Using automated imaging, computer controlled scanning electron microscopy (CCSEM) can provide quantitative results within a reasonable analysis time. Because of this automation, microscopy has entered a new era. CCSEM permits comparison of microscopic results with those from bulk analyses while retaining the feature specific resolution of manual microscopy. The replicability, precision, and accuracy of CCSEM were recently evaluated during a study for the Texas Air Control Board. Elemental concentrations obtained by CCSEM were compared with those from several bulk analysis methods. The CCSEM results were determined to be quantitative. The environmental applications of CCSEM described in this paper are: a) determination of equivalent aerodynamic diameters, b) air particulate sampler inlet modeling, c) source emission characterization, and d) receptor modeling.

The microscope, in all its forms, has been an important scientific tool for four centuries. Using a rudimentary compound optical microscope, Anton van Leeuwenhoek (1632–1723) was able to view bacteria and other single cell organisms. He also played a key role in the controversy surrounding spontaneous generation, by observing that insects develop from eggs laid in mud.[1] Since that time, improvements in optical light microscopy have included design modifications and development of techniques such as dispersion staining and phase contrast which aid in feature resolution and identification. However, the theory of image formation developed by Abbe near the end of the nineteenth century predicted an ultimate resolution for the light microscope of about 0.2 μm, limited by the wavelength of light.[2] The practical resolution of the light microscope is more typically about 1–2 μm. The desire to obtain additional resolution of microscopic features inspired experimentation with the use of electrons in the early 1900s. Developments in electronics eventually resulted in the construction of the first successful electron microscope in 1932. During the past 50 years, electron microscopy has evolved to include the transmission electron microscope (TEM), the scanning electron microscope (SEM) and the scanning transmission electron microscope (STEM). The use of electrons to form magnified images provides feature resolution as great as a few angstroms.

Both optical and electron miscroscopy have been widely used in environmental studies of particulate matter. Until recently, however, the information obtained from these techniques has usually been qualitative because of the limited number of particles counted. Early image analysis techniques provided more rapid particle counting.[3] However, to obtain a quantitative analysis, particles must be properly sized and identified by chemistry and/or morphology in sufficient numbers to be representative of the entire sample. In this manner, the microscopic characteristics can be directly and reliably related to the bulk or macroscopic properties of the sample. With the proliferation of the microcomputer, microscopy has entered a new era. The use of the microcomputer has enabled the collection of individual particle data in a fashion which permits comparison with the macroscopic properties of the sample while retaining the particle specific resolution. Today, many environmental studies are incorporating the use of automated scanning electron microscopy.[4–8] This method of analysis, referred to as computer controlled scanning electron microscopy (CCSEM), provides simultaneous measurement of individual particle size, shape and elemental composition. This paper briefly describes how CCSEM works, discusses its strengths and limitations, and illustrates how it is being used in environmental studies.

Computer Controlled Scanning Electron Microscopy

CCSEM combines three analytical tools under computer control: 1) the scanning electron microscope, 2) the energy dispersive spectrometry X-ray analyzer, and 3) the digital scan

Table I. Comparison of CCSEM results from replicate analysis (Wt. %).

Particle type	Original analysis	Replicate analysis
Si-rich	6.7	7.1
Ca-rich	19	20.6
Fe-rich	2.6	2.1
Ca-Si	23.2	21.4
Pb-rich	6.1	6.3
Pb-Br	1.3	2.3
Pb-bearing	3	3.4

The volume of each particle, computed from the projected area measurements, is multiplied by the particle density to obtain the particle's mass.

An example of the type of individual particle information that is acquired with CCSEM is illustrated in Figure 1. The top pictures are secondary electron micrographs of two particles (note difference in morphologies). The calcium amphibole particle is naturally occurring, while the cenosphere (round flyash) particle is the result of a combustion process. The middle pair of micrographs are backscattered images of each particle. The superimposed diagonals on each particle illustrate how average particle size and shape are determined. The bottom pictures show the elemental X-ray spectra from the particles.

Table II. Precision of CCSEM elemental results.

Elemental concentration (Wt. %)	Average relative error (%)	95 percent confidence interval (%)
<1	35	0.65–1.35
2.5	32	1.94–3.06
5	16	4.36–5.64
10	8	8.8–11.2
>15	5	14.3–15.7

Advantages and Disadvantages of CCSEM

CCSEM, like most analytical techniques, possesses both advantages and disadvantages. These are as follows:

Advantages

- Particle size may range from 0.2–300 μm.
- Elemental chemistry is obtained from each particle.
- Particles are classified by elemental composition and morphology.
- Analysis time averages two seconds for each particle.
- Mass and frequency distributions are obtained for each particle class as a function of size.
- Both physical (geometric) and aerodynamic particle size are determined.
- Data from each particle are permanently stored.
- The analysis is compatible with most sampling methods and filter media.
- Effects of operator bias, fatigue and subjectivity, inherent in manual microscopy, are eliminated.
- Results are reproducible, and compare favorably with other analytical methods.

Disadvantages

- Most filter samples require redeposition to separate and disperse the particles.
- Sample changes may be induced by the redeposition process.
- Particles with an atomic number close to that of the filter substrate are difficult to detect.
- Particle volume is inferred from the projected area.
- Particle mass is calculated using a density that is assumed to correspond to the particle type.
- Chemical inhomogeneities within a particle may not be recognized.
- Particles yielding few or no detectable X-rays are assumed to be carbonaceous.

Precision and Accuracy of CCSEM

The ability of CCSEM to rapidly analyze large numbers of particles overcomes many of the limitations inherent with manual microscopic methods.[15] Because the analysis of each particle by CCSEM is accomplished in about two seconds, large numbers of particles can be analyzed in a relatively short period of time. Computer control of the SEM also enables each particle to be tested against the same set of analysis parameters, assuring uniformity of the analysis. CCSEM results have been shown to be more precise and accurate than commonly employed manual methods.[16]

Examples of the replicability, precision, and accuracy of CCSEM results are illustrated in Tables I through III. Table I, presenting selected particle type results from the analysis of a cellulose filter, illustrates the replicability of the CCSEM analysis. The replicate analysis was obtained by preparing a different section of the original sample. As can be seen, there is very good agreement for all particle types. Generally, the relative error decreases as the elemental concentration increases, as illustrated in Table II. This table presents the average relative errors based on CCSEM results from 17 replicate samples. The results are presented at the 95% confidence level. On average, there is a relative error of 35% for elements that account for less than 1 weight percent, and a relative error of 5% for elements contributing more than 15 weight percent. Since the replicate samples were prepared from a different

Table III. Comparison of elemental concentrations from analyses of collocated and replicate filters (% TSP).

	Glass fiber filter					Cellulose filter					Replicate cellulose				
Element	AA	XRF	PIXE	CCSEM	IC	AA	XRF	PIXE	CCSEM	IC	AA	XRF	PIXE	CCSEM	IC
Si	[b]	[a]	0	10.5	[b]	[b]	6.9	11.8	10.1	[b]	[b]	[b]	10.3	9.6	[b]
S	[b]	[a]	3.1	1.7	3.3	[b]	4.2	3.2	2.8	2.1	[b]	[b]	2.9	2.1	2
Ca	[b]	[a]	10.3	12.5	[b]	[b]	11.9	10.7	10.8	[b]	[b]	[b]	9.6	10.8	[b]
Fe	[b]	[a]	2.1	3.3	[b]	[b]	2.3	2.6	3	[b]	[b]	[b]	2.4	2.3	[b]
Pb	2.1	2.2	2.3	1.3	[b]	[b]	2.6	2.6	2.5	[b]	[b]	[b]	2.6	2.7	[b]
Br	[b]	0.3	0.3	0.7	0.7	[b]	1.2	0.9	0.6	0.4	[b]	[b]	0.8	1.1	0.4
Zn	1.1	[a]	1	0.8	[b]	[b]	1	1.2	0.8	[b]	[b]	[b]	1.1	1	[b]

[a] Not reported
[b] Not analyzed.

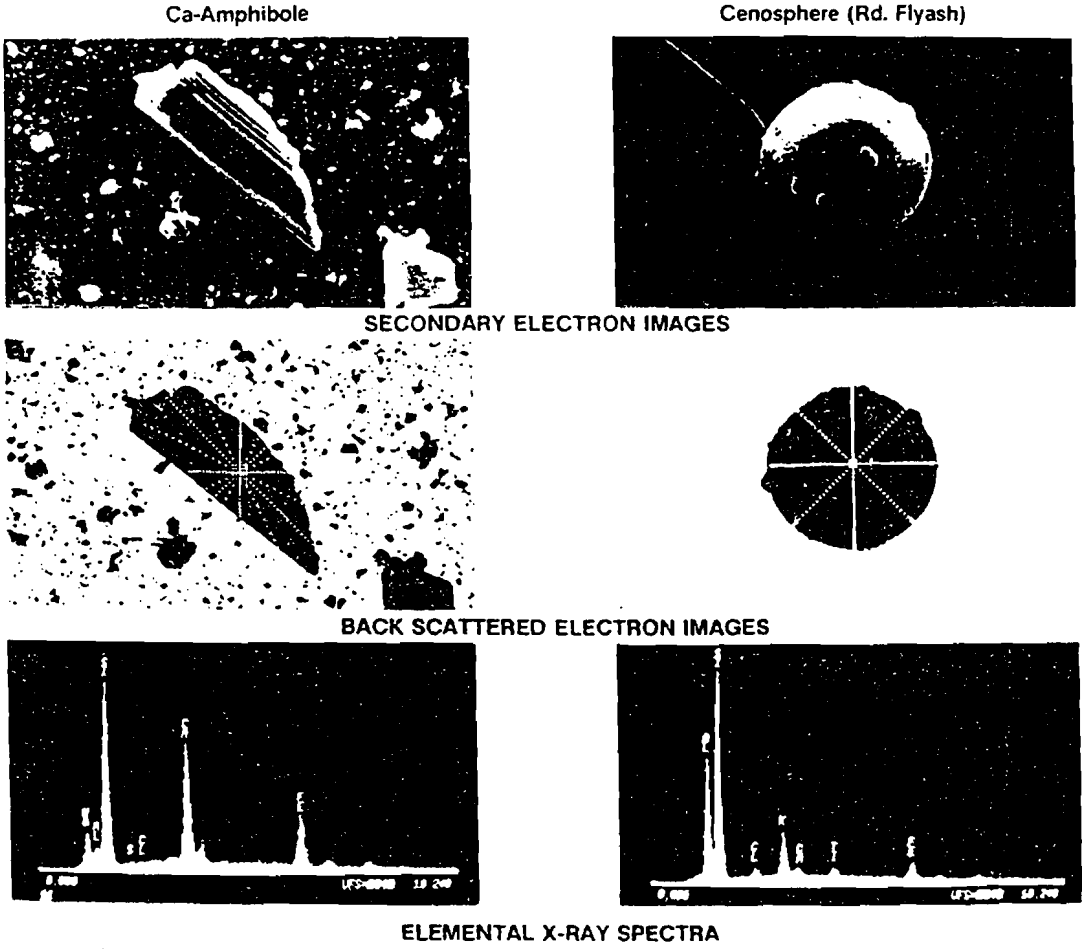

Figure 1. Pictorial demonstration of typical CCSEM analyses of ambient air particles.

generator for image processing. In the SEM, a finely focused electron beam impinges upon the sample surface. The interaction of the electron beam with the sample produces various effects that can be monitored with suitable detectors. Some of these effects include the production of secondary, backscattered and Auger electrons; emission of characteristic X-rays; photo and cathodoluminescence; and electron channeling. Most commonly, secondary and/or backscattered electrons are used to create a viewing image, while the X-ray emission is monitored to determine the elemental chemistry of features of interest.

In air particulate studies, the automated image analysis generally uses the backscattered electron mode, which is sensitive to differences in atomic number, to determine when the beam is on a particle. As the computer moves the electron beam across the image, the image intensity at each point is compared with a threshold level. This comparison is used to determine whether the electron beam is "on" a particle (above threshold) or "off" a particle (below threshold). If the signal is below the threshold level, the computer selects a new coordinate and directs the beam to the new point. The distance between these "off points" is specified so that all particles larger than a selected size will be detected. Once a coordinate is reached where the signal is above the threshold level, the computer switches to a subroutine that drives the beam across the particle in a preset pattern to determine the dimensions and shape of the detected feature. For each feature, the maximum, minimum, and average diameters are stored, along with the centroid location. The centroid of each particle is compared with those of previously detected particles to prevent double counting. More detailed descriptions of automated imaging in the scanning electron microscope have been presented elsewhere.[9-14]

CCSEM classifies each particle as a particle type based on its elemental chemistry. This is accomplished by collection of characteristic X-rays which are fluoresced by the electron beam on the particle. The X-ray spectrum from each particle is processed to obtain relative concentrations for the following 19 elements: Na, Mg, Al, Si, P, S, Cl, K, Ca, Ti, V, Cr, Mn, Fe, Cu, Ni, Zn, Pb, and Br. Using the chemistry and shape factor, each particle is assigned to a defined particle type. If a particle's chemistry fits none of the predefined types, a new type can be created. The absence of elemental peaks, or a low peak to background ratio, causes the particle to be classified as carbon. It should be noted that the labels assigned to particle types are often descriptors of elemental composition and do not imply positive identification of a specific chemical compound. For example, metallic iron, iron oxides, and iron carbonates occupy the iron-rich category. Based on the most likely chemical compound(s) represented by the observed particle properties, each particle type is assigned a density.

Cover Photograph. Spatial distribution of elements within a lead-bearing particle, obtained by CCSEM. Digital processing of the X-ray signal was performed on a Tracor Northern image processing system. Left: Intensity maps of the characteristic X-rays for each of the four elements—lead (red), chlorine (green), tin (blue), and calcium (gold). Right: Composite elemental map of the same particle (at twice the magnification), produced by combining the maps of three elements—lead, chlorine, and tin. Where two or more elements are present, a new color results: lead and chlorine (yellow), lead and tin (magenta).

Table IV. Comparison of physical and aerodynamic size distributions in a coal-fired boiler sample.

Particle Type	Diameter (μm) 0.2–2.5	2.5–5	5–10	10–15	15–30	>30	Total (Wt. %)
Weight distribution, physical diameter range							
Cenosphere	25	25	36	8	6	0	32.6
Quartz	2	14	40	18	25	0	9.4
Fe-rich	2	39	34	25	0	0	3.1
Round-Fe	18	37	32	13	0	0	6
Mix-clay	6	26	36	17	14	1	39.2
Carbon	4	9	0	47	40	0	2.8
Fe-Si	15	19	30	28	9	0	2.7
Miscellaneous	14	23	27	20	16	0	4.3
Total	13	25	35	15	12	1	100
Weight distribution, aerodynamic diameter range							
Cenosphere	9	24	33	19	15	1	32.6
Quartz	0	4	19	29	37	11	9.4
Fe-rich	2	0	28	46	25	0	3.1
Round-Fe	2	3	43	38	13	0	6
Mix-clay	2	10	33	19	26	10	39.2
Carbon	4	3	6	7	80	0	2.8
Fe-Si	3	17	30	13	37	0	2.7
Miscellaneous	10	9	27	18	31	5	4.3
Total	5	13	31	21	25	6	100

section of the original filter, the results also include any influences that sample preparation may have on precision.

Elemental results obtained from CCSEM and various bulk chemistry methods are presented in Table III. The analytical methods compared with CCSEM in this table include: atomic absorption (AA), bulk X-ray fluorscence (XRF), proton induced X-ray emission (PIXE), and ion chromatography (IC). The glass fiber and cellulose filters were obtained from collocated hi-vol samplers. A replicate analysis (from another section of the original filter) was performed on the cellulose sample. Because the TSP concentrations from the glass fiber filter (156 $\mu g/m^3$) and the cellulose filter (111 $\mu g/m^3$) were significantly different, elemental results are presented as a percent of TSP. For the XRF method, only heavier elemental results were reported from the glass fiber filter because of interferences from the filter matrix. Replicate XRF analysis was not performed on the cellulose filter. AA was performed only on the glass fiber filter, while PIXE, CCSEM and IC results were performed for all samples. The results in this table generally show good agreement between methods. The PIXE results for silicon (Si) illustrate the difficulties encountered by bulk methods in correcting for interferences from elements present in the glass fiber filter. CCSEM was capable of measuring the silicon content of the TSP because it can recognize and reject the filter particles from the analysis. Results for sulfur (S) showed that CCSEM reported a lower value than PIXE and IC for the glass fiber filter. The sulfur results from the cellulose filter show better agreement between IC and CCSEM. The lead (Pb) results show good agreement for all methods with the exception of CCSEM reporting a lower value on the glass fiber filter.

Environmental Applications of CCSEM

One of the earliest environmental applications of CCSEM was the identification of sources contributing to TSP concentrations.[17] With continued development, the role CCSEM plays in environmental studies has expanded to encompass additional applications. The CCSEM applications discussed in this paper include: a) determination of equivalent aerodynamic diameter, b) air sampler inlet modeling, c) source emission characterization, and d) receptor modeling.

Determination of Equivalent Aerodynamic Diameter

The importance of the size distribution of suspended particulate matter has taken on new significance in light of a possible size specific standard. At this writing, a thoracic particulate (TP) standard will most likely be proposed based on the fraction of the aerosol components that are believed to enter the human respiratory system. Monitoring would be conducted with samplers having a cut point based on aerodynamic size. As a part of the CCSEM analysis, both number (frequency) and weight distributions of the particulate matter sample are determined. To convert a measured physical diameter to an equivalent aerodynamic diameter, an approximation can be made, based on the particle's density, physical diameter and shape. The equation used by CCSEM to calculate the equivalent aerodynamic diameter is:

$$D_a = \chi D_p(\rho)^{1/2} \quad (1)$$

where D_a = equivalent aerodynamic diameter
χ = aerodynamic shape factor
D_p = physical diameter
ρ = particle specific gravity

This aerodynamic conversion was recently validated by comparing the CCSEM aerodynamic size distributions with results obtained by more conventional aerodynamic size measurement methods.[18]

Table IV provides a comparison of the physical and aerodynamic size distributions for various particle types found in

Table V. Inlet modeling results averaged by type of mining operation.

Operation	TSP	TP – D_0	TP – D_{50}	$\frac{TP - D_0}{TSP}$	$\frac{TP - D_{50}}{TSP}$	$\frac{TP - D_{50}}{TP - D_0}$
Silver	242.9	59.1	103.2	0.24	0.43	1.77
Molybdenum	148.9	26.1	53.2	0.15	0.33	2.22
Copper	174.6	29.5	58.4	0.17	0.33	2.02
Coal I	126.4	24.3	48.2	0.19	0.37	2.08
Coal II	214.3	33.5	78.1	0.13	0.31	2.41
All	180.7	34.2	67.8	0.18	0.35	2.1

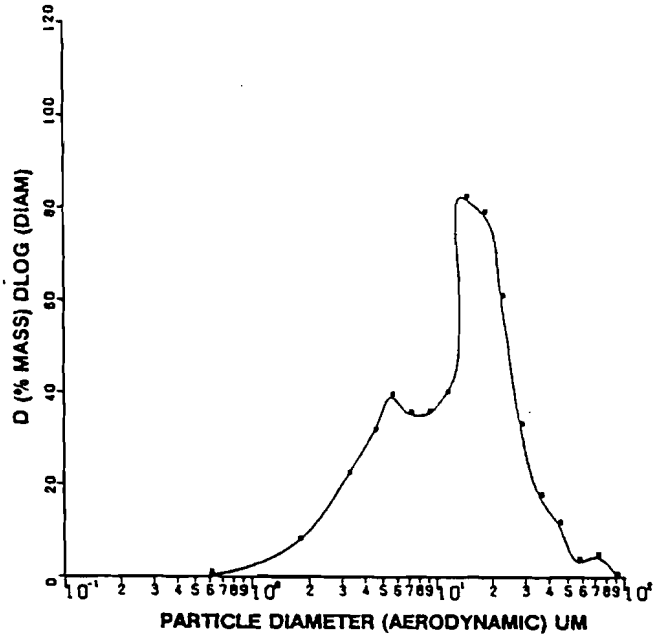

Figure 2. Graphic illustration of the aerodynamic distribution collected at a silver mining operation.

a coal-fired boiler stack. For this sample, the equivalent aerodynamic diameter is slightly larger than physical diameter. An example of the variability in the aerodynamic size distribution of particulate matter collected by the hi-vol is illustrated in Figures 2 and 3. Figure 2 shows a pronounced bimodality, with the majority of the mass around 12 μm. Figure 3, from a different geographic area, shows no evidence of bimodality. In both figures, note the decrease in mass occurring around 30 μm. The steep slope may reflect the poor collection characteristics of the hi-vol sampler for particles larger than 30 μm.[19]

Inlet Modeling

The relative mass fraction that would be collected by a size selective sampler may be predicted from the sampler inlet effectiveness curve and the aerosol particle size distribution. Although this application of inlet modeling is relatively new, EPA has been examining the possible use of a multiplier to convert hi-vol TSP measurements to estimate the concentration of respirable particulate matter.[20–22] An EPA document[23] has reported that a 0.5–0.6 factor is expected to convert TSP to TP in typical urban areas. As the appropriate size inlet for the collection of TP is currently being reviewed by EPA, additional information regarding the relationship between sampling devices is needed.

In a study of surface mining operations, an inlet model that incorporated aerodynamic size results from CCSEM analyses was used to convert TSP to TP concentrations.[24] The results from this inlet modeling study, averaged by mining operation, are presented in Table V. The estimated TP/TSP ratios suggest that a conversion factor applied to areas around surface mining operations should be lower than the reported EPA values for typical urban areas. Overall, the average TP/TSP ratio was 0.18 for a 10 μm D_0 inlet and 0.35 for a 10 μm D_{50} inlet. A 10 μm D_0 sampler is one which theoretically will exclude all particles which have an aerodynamic diameter greater than 10 μm. A 10 μm D_{50} sampler is one which ideally has a 50% probability of collecting 10 μm particles, and has a lower probability of collecting larger particles. Results of the study indicate that TP/TSP ratios vary by geographic location, monitoring site, and in some instances, by TSP loading.

Source Characterization

In source characterization studies, CCSEM is used to measure the relative distributions, in different size ranges, of particle types generated by a specific source. This information is often used to evaluate the effectiveness of emission control devices. Table VI shows results from the analysis of particulate matter collected in a lime kiln stack. Referring to this table, the lime kiln is characterized mainly by calcium-rich, calcium-silicon and halide particles. The difference in emissions from various sources is illustrated by comparing the

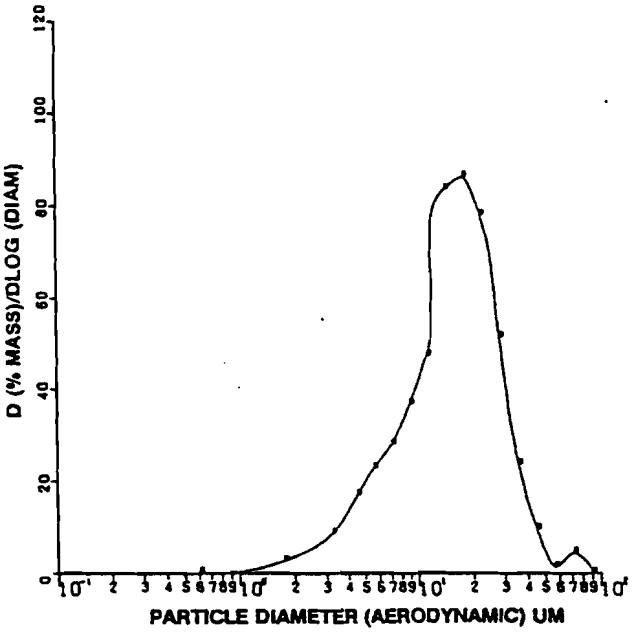

Figure 3. Graphic illustration of the aerodynamic distribution collected at a coal mining operation.

Table VI. CCSEM results from lime kiln stack sample.

Particle Type	Diameter (μm) 0.2–2.5	2.5–5	5–10	10–15	15–30	>30	Total (Wt. %)
Weight distribution, aerodynamic diameter range							
Silicon-Rich	1	8	25	16	50	0	3.7
Calcium-Rich	1	9	37	20	32	1	44.5
Calcium-Sulfur	3	25	60	12	0	0	1.1
Magnesium-Calcium	2	8	41	13	37	0	8.3
Halide (K-Cl)	9	9	11	12	47	4	11.6
Mix-Clay	4	13	13	12	57	0	2.5
Calcium-Silicon	3	7	29	26	35	0	13.6
Carbon	5	23	19	19	15	19	2.2
Miscellaneous	5	17	21	5	36	15	12.5
Total	2	10	30	18	36	3	100

Table VII. Fingerprint/ratio source apportionment results for TSP and lead-bearing particles at various monitors in El Paso; results presented at the 95% confidence interval.

Monitor site	Average concentration ($\mu g/m^3$)	Number of samples	Urban soil (%)	Industrial fugitives (%)	Highway (%)	Smelter (%)	Unknown (%)
			Total Suspended Particulates				
A	131	10	50–54	17–21	9–13	8–12	9–11
B	147	9	53–59	15–19	10–16	5–7	8–10
C	76	4	55–65	11–17	5–11	6–12	7–11
D	80	4	78–92	2–4	6–12	3–5	3–5
E	311	12	45–49	21–25	2	17–25	6–9
F	91	8	75–83	7–9	2–4	7–11	7–9
G	78	8	54–60	4	13–21	3–5	9–13
			Lead-Bearing Particles[a]				
A	6.1	10	2	0	12–20	47–71	18–22
B	6.7	9	4	0	22–35	33–51	23–27
C	2.9	4	1	0	6–14	57–100	1
D	2.5	4	8	0	27–52	22–48	16–22
E	29.9	12	4	0	2–4	64–94	15–19
F	1.1	8	17–19	0	13–21	49–79	8–10
G	1.6	8	1	0	37–63	31–51	8–10

[a] Includes all particles that have lead composition, not elemental lead.

analysis results from the lime kiln with those from the boiler house in Table IV. As can be seen, the boiler house emissions are comprised mainly of mix-clay and cenosphere particle types. Source characterization has also been used to define the source "fingerprint" or "signature" in receptor modeling studies.

Receptor Modeling

Mathematical models have been developed to estimate the impact of emission sources on ambient air quality. Dispersion models are source oriented, predicting ambient concentrations from measured source strengths. Receptor models, however, characterize ambient samples to identify the sources and to quantify their contribution. Receptor models have attracted interest as a possible tool to validate dispersion models.[25,26] Presently, a variety of receptor modeling techniques exist, incorporating data generated by a number of analytical methods.[27] For air particulate studies, these analytical methods are generally divided into two categories: macroscopic methods based on bulk chemical analysis, and microscopic methods based on individual particle analysis. Each type of model has certain advantages and disadvantages.[28] However, models which use microscopic data presently show the most promise for resolving specific source impact.[29]

The fingerprint/ratio receptor model, developed over the past three years, utilizes the size, shape and chemistry data from CCSEM to apportion the sources of particulate matter. The ratios of particle type concentrations at the source(s) are fitted to those found at the ambient monitor, using a least squares procedure. This fitting process is performed separately for various size ranges, in an attempt to account for particle deposition between source and receptor. In two studies employing the fingerprint/ratio receptor model, the source apportionment results were used to evaluate the Industrial Source Complex (ISC) dispersion model.[4,30] An important feature of the ISC model is that it was designed to calculate particle deposition. A comparison of the receptor and dispersion model results showed good agreement when CCSEM size distributions of sources were used in the ISC model.

Recently, the Texas Air Control Board conducted a study to identify and quantify sources of TSP and particulate lead in El Paso.[31] To accomplish this goal, CCSEM and the fingerprint/ratio receptor model were selected as the primary methods. The CCSEM analyses and fingerprint/ratio results correlated well with results from other analytical methods and receptor models. Fingerprint/ratio results from the seven monitors studied are summarized at the 95% confidence level in Table VII. The source apportionment results indicated that soil and industrial fugitive emissions accounted for the majority of the TSP. As expected, smelter and automotive emissions accounted for the majority of the lead-bearing particles.

Summary and Future Research

During the past five years, CCSEM has become recognized as an extremely powerful analytical tool. The use of CCSEM to ascertain specific particulate information in environmental studies will enable scientists to evaluate data in a more sophisticated manner. Because CCSEM can obtain size related information, this technique may become more widely used to elucidate the health effects aspects of particulate matter. As a result of this technology, the field of environmental science will be able to explore areas not accessible by most other analytical methods.

Acknowledgments

The authors gratefully acknowledge valuable assistance and discussion provided by Dr. Robert M. Fisher and the electron optics group of U.S. Steel Research Laboratories. We also wish to thank the Texas Air Control Board for their input and assistance. Many thanks to Lin Cole and Stanley Lentz for their assistance in preparing this manuscript.

References

1. J. R. Meyer-Arendt, *Introduction to Classical and Modern Optics*, Prentice-Hall, Inc., 1972, p. 133.
2. J. W. S. Hearle, J. R. Sparrow, P. M. Cross, *The Use of the Scanning Electron Microscope*, Pergamon Press, 1972, p. 1.
3. R. R. Irani, C. F. Callis, *Particle Size: Measurement, Interpretation and Application*, John Wiley & Sons, Inc., 1963, p. 102.
4. J. H. Lucas, "A Comprehensive Study of Particulate Emissions from an Integrated Iron and Steel Plant to Aid in the Design of a Control Strategy Program," in *Air Pollution Control in the Iron and Steel Industry*, SP-40, Air Pollution Control Association, Pittsburgh, PA, 1979.
5. J. R. Zwikl, P. E. Kueser, A. Roffman, L. L. Simmons, "An Alternative Emission Control Plan for Industrial Plants—Birth of a Concept and its Regulatory Implications," presented at the 74th Annual Meeting of the Air Pollution Control Association, Philadelphia, PA, 1979.
6. P. B. Janocko, G. S. Casuccio, S. L. Dattner, D. L. Johnson, E. R. Crutcher, "The El Paso Airshed; Source Apportionment Using Complementary Analyses and Receptor Models," in *Receptor*

Models Applied to Contemporary Pollution Problems, SP-48, Air Pollution Control Association, Pittsburgh, PA, 1982.
7. D. L. Johnson, B. L. McIntyre, R. Fortmann, R. K. Stevens, R. B. Hanna, "A chemical element comparison of individual particle analysis and bulk analysis methods," *Scanning Electron Microsc.* 1: 469 (1981).
8. B. L. McIntyre, D. L. Johnson, "A Particle Class Balance Receptor Model for Aerosol Apportionment in Syracuse, N.Y.," in *Receptor Models Applied to Contemporary Pollution Problems*, SP-48, Air Pollution Control Association, Pittsburgh, PA, 1982.
9. J. J. McCarthy, "Applications of a Digital Scan Generator to EDS Analysis," in *Microbeam Analysis*, D. E. Newbury, ed., San Francisco Press, San Francisco, CA, 1979.
10. R. J. Lee, J. F. Kelly, "Back-Scattered Electron Imaging for Automated Particle Analysis," *Microbeam Analysis*, D. E. Newbury, ed., San Francisco Press, San Francisco, CA, 1979.
11. M. R. Hoover, E. W. White, J. Lebiedzik, G. G. Johnson, Jr., "Automated Characterization of Particulates and Inclusions by Computer Controlled SEM Probe," Proceedings of the 10th Annual Microbeam Analysis Society Conference, 1975.
12. W. R. Scott, E. J. Chatfield, "A precision SEM image analysis system with full feature EDXA characterization," *Scanning Electron Microsc.* 2: 53 (1979).
13. R. J. Lee, J. F. Kelly, "Applications of SEM-Based Automated Image Analysis," *Microbeam Analysis*, D. B. Wittry, ed., San Francisco Press, San Francisco, CA, 1980.
14. R. J. Lee, J. F. Kelly, "Overview of SEM-based automated image analysis," *Scanning Electron Microsc.* 1: 303 (1980).
15. R. J. Lee, W. A. Spitzig, J. F. Kelly, R. M. Fisher, "Quantitative metallography by computer controlled scanning electron microscopy," *J. Metals* 33: 3 (1981).
16. R. J. Lee, R. M. Fisher, "Quantitative Characterization of Particulates by Scanning and High Voltage Electron Microscopy," National Bureau of Standards Special Publication 533, 1980.
17. R. J. Lee, E. J. Fasiska, P. B. Janocko, D. G. McFarland, S. J. Penkala, "Electron-beam particulate analysis," *Industrial Res. Dev.*, June 1979.
18. P. B. Janocko, G. S. Casuccio, R. L. Kerch, "The Use of Automated Microscopy to Estimate Thoracic Particulate Levels from Hi-Vol Filter Measurements," in *Fugitive Dust Issues in the Coal Use Cycle*, SP-51, Air Pollution Control Association, Pittsburgh, PA, 1983.
19. A. R. McFarland, C. A. Ortiz, C. E. Rodes, "Characteristics of Aerosol Samples used in Ambient Air Monitoring," presented at the 86th National Meeting of the American Institute of Chemical Engineers, Houston, TX, 1979.
20. J. G. Watson, J. C. Chow, J. J. Shaw, "Analysis of Inhalable and Fine Particulate Matter Measurements," Final Report to the Environmental Protection Agency by Environmental Research and Technology under contract No. 68-02-2542, pp. 2–29, December 1982.
21. T. G. Pace, "Estimating PM_{10} Concentrations from IP and TSP Data," presented at the 75th Annual Meeting of the Air Pollution Control Association, New Orleans, LA, 1982.
22. J. G. Watson, J. C. Chow, J. J. Shaw, T. G. Pace, "The effect of sampling inlets on the PM-10 and PM-15 to TSP concentration ratios," *JAPCA* 33: 114 (1983).
23. "Review of the National Ambient Air Quality Standards for Particulate Matter: Assessment of Scientific and Technical Information," Report No. EPA-450/5-82-001, p. 107, U.S. Environmental Protection Agency, January 1982.
24. J. P. Constantino, P. B. Janocko, G. S. Casuccio, R. L. Kerch, "Thoracic Particulate Levels at Surface Mining Operations Determined by Automated Microscopic Analysis of Hi-Vol Filters," in *Fugitive Dust Issues in the Coal Use Cycle*, SP-51, Air Pollution Control Association, Pittsburgh, PA, 1983.
25. J. E. Core, W. M. Cox, "Particulate Dispersion Model Evaluation: A New Approach Using Receptor Models," presented at the 75th Annual Meeting of the Air Pollution Control Association, New Orleans, LA, 1982.
26. P. L. Hanrahan, "Improved Particulate Dispersion Modeling Results: A New Approach Using Chemical Mass Balance," presented at the 74th Annual Meeting of the Air Pollution Control Association, Philadelphia, PA, 1981.
27. "Receptor Model Technical Series Volume I: Overview of Receptor Model Application to Particulate Source Apportionment," Report No. EPA-450/4-81-016a, U.S. Environmental Protection Agency, July 1981.
28. J. E. Core, T. G. Pace, "Receptor Models—How Great Thou Art!(?)," presented at the 74th Annual Meeting of the Air Pollution Control Association, Philadelphia, PA, 1981.
29. J. A. Cooper, J. G. Watson, Jr., "Receptor oriented methods of air particulate source apportionment," *JAPCA* 30: 1116 (1980).
30. G. S. Casuccio, J. H. Lucas, P. B. Janocko, "A Comparison of the Particulate Matter Emission Inventory to Dispersion Modeling and Receptor Results at the Coke and Iron Division of Shenango Incorporated," in *Emission Inventories and Air Quality Management*, SP-46, Air Pollution Control Association, Pittsburgh, PA, 1982.
31. "Identification of the Sources of Total Suspended Particulates and Particulate Lead in the EL Paso Area by Quantitative Microscopic Analysis—Vols. I & II," Final report prepared for the Texas Air Control Board, Austin, Texas, by Energy Technology Consultants under Contract No. 5400-030 AIR 2-1774, March 1983.

The authors are affiliated with the following: Mr. Casuccio and Mr. Janocko, Energy Technology Consultants/Atmospheric Research Organization, Inc., 4758 Old William Penn Highway, Murrysville, PA 15668; Dr. Lee and Dr. Kelly, United States Steel Research Center, 125 Jameson Lane, Monroeville, PA 15235; Mr. Dattner and Mr. Mgebroff, Texas Air Control Board, 6330 Highway 290 East, Austin, TX 78723. This report is based on paper number 82-21.4, presented at the 75th APCA Annual Meeting and Exhibition in New Orleans, June 1982.